# DEVELOPMENT OF A THEORY OF THE SPECTRAL REFLECTANCE OF MINERALS

## PART III

*by*

J. R. ARONSON, A. G. EMSLIE, L. H. ROACH, E. M. SMITH, and P. C. von THŰNA

JANUARY 1, 1972

NAS 9-10875

ADL C-72594





Arthur D. Little, Inc.

# DEVELOPMENT OF A THEORY

# OF THE SPECTRAL REFLECTANCE OF MINERALS

# PART III

By

J. R. Aronson, A. G. Emslie, L. H. Roach,
E. M. Smith, and P. C. von Thüna

Prepared for

National Aeronautics and Space Administration
Manned Spacecraft Center
Houston, Texas 77058

Interim Technical Summary Report

Contract NAS 9-10875

ADL C-72594

January 1, 1972

Arthur D. Little, Inc.

## Abstract

Further significant refinements have been made in the theory of the diffuse reflectance of particulate media. The theory now correctly predicts the opposite trends of reflectance with particle size in regions of the spectrum in which the particles are semi-transparent and those in which they are opaque. The mechanism required for this improvement is that of enhanced absorption caused by wave-optical effects of small surface asperities and edges. The same mechanism remedies the theory to account for the previously mysterious behavior of the data in spectral regions of anomalous dispersion.

## Table of Contents

## LIST OF FIGURES

## LIST OF FIGURES (Continued)

# I. INTRODUCTION

At the conclusion of our previous work[1], the development of the theory of spectral reflectance (emittance) of mineral powders had progressed to the stage that the general spectral shape and certain particle size trends were reasonably well predicted. Specifically, the results shown in Figure 12 (for quartz) and Figure 18 (for corundum) in our last report[1] indicated that the particle size trends predicted by theory were in agreement with the experimental results in regions of the spectrum in which the particles are semitransparent. As can also be observed in these figures, the general shapes of the spectra were well predicted. Further, the same sorts of agreement were found for garnet and glass powders and a mixture of quartz and corundum.

The principal discrepancies between theory and experiment were:

1. The inadequate prediction of the particle size trends in spectral regions of high particle opacity
2. The failure of the theory to predict the spectral shape for corundum in the region of anomalous dispersion, i.e., between 660 and 860 $cm^{-1}$. See Figure 18 of the last report. (We refer to this shape as a "scallop" taken out of the "single crystal shape.")
3. The improper prediction of the level of the spectrum by either the coarse- or the fine-particle theory in the regime where the particle size is comparable to the radiation wavelength. See Figure 14 of the aforementioned report[1].

During the course of the work carried out during the present report period, we have directed the experimental program at resolving these discrepancies. The results to be presented in this report have provided the clues that led us to make certain revisions in the theory, which, as will be seen, have largely removed the problems.

It was always recognized that the most difficult part of the theoretical model would occur in the particle size regime that approximates the radiation wavelength. We have long felt that a geometrical-optics approach would be quite satisfactory for relatively large particle sizes, and that a wave-optics approach, such as discussed in our previous work[1,2] based on a Lorentz-Lorenz type of treatment, would be proper for very fine particles. After each of these treatments was fully developed, we felt a semiempirical bridging of the two theories would suffice to cover the entire range of particle sizes. The essential correctness of our coarse-particle model was apparent in previous reports and at various times our fine-particle model appeared to approximate the experimental results. However, in each example of the use of the fine-particle model to fit experimental data (where, in fact, the data pertained to the difficult particle-size regime mentioned above), we retained some reservations on the approximations involved or found certain serious discrepancies in selected spectral regions. For instance, the Lorentz-Lorenz treatment and its subsequent modifications predicted, in conflict with experiment, the existence of a strong surface reflectance in certain spectral regions resulting from the discontinuity in the average optical properties at the boundary of the particulate medium. In view of these difficulties with the applicability of the fine-particle model to the particle size range with which the experiments dealt, it seemed appropriate to bypass the fine-particle theory and in its place to extend the coarse-particle theory by the addition of certain wave optical modifications. In support of this concept, we refer to the rather good agreement shown in our last report (Figure 16)[1] between our coarse-particle model and the Mie Theory calculations of Conel[3]. At even lower particle sizes than shown in the figure, the two theories had some qualitative agreement. It should be noted that neither theory predicts the distinct reduction in reflectance with decreasing particle size that is observed in opaque regions for $d/\lambda$ ratios varying from 30 down to one. This inadequacy of both theoretical treatments strongly suggested that an extraordinary mechanism for absorption is involved.

The scallop-shaped spectral feature referred to above also suggests an additional absorption mechanism which is not predicted by either of the theories. In this case the enhanced absorption seems to be superimposed on the extra absorption found generally in opaque regions and occurs for a certain restricted range of the optical constants of the particles.

Now it is well known that enhanced absorption relative to scattering occurs for opaque particles that are much smaller than the wavelength, as with gold and other metallic blacks. This effect is predicted by the induced dipole approximation first derived by Lorentz[4]. The Lorentz dipole effect is thus seen to be a very attractive explanation of the puzzling phenomena of enhanced absorptions. However, owing to the large size of the particles in which these phenomena still occur (viz, 120μ corundum), invoking the dipole hypothesis presents an apparent paradox. The reason is that the induced polarization in a particle that is many wavelengths in diameter must be represented as a high order multipole rather than a simple dipole. Such a multipole does not produce a large absorption to scattering ratio. The resolution of this dilemma constitutes the main contribution of the present report.

Another possible mechanism for enhanced absorption is that provided by non-uniform packing density or aggregation in the powder. It is easy to show that a clump of opaque particles has a lower reflectance than an individual particle. Therefore, the diffuse reflectance of a semi-infinite medium composed of uniformly distributed clumps has a lower diffuse reflectance than a uniform distribution of individual particles. A similar problem has been treated in detail by Giovanelli[5]. We will attempt to distinguish the effects of this mechanism from the dipole hypothesis mentioned above.

## II. IDENTIFICATION OF ASPERITIES AS THE SOURCE OF THE DIPOLE ABSORPTION MECHANISM

The most critical experimental evidence bearing on the dipole paradox posed in the introduction is to be found in the set of spectra of spherical glass beads shown in Figure 1. The vital point to be observed in this figure is the excellent agreement between theory and experiment for this material. We particularly note the correct theoretical prediction of the particle size trends in the opaque regions of the spectrum near 450 $cm^{-1}$ and 1050 $cm^{-1}$. The level is excellently predicted as well and the agreement is in marked contrast with the inadequate theoretical prediction for quartz and corundum particles of the same size range (See Figures 12 and 18 of our last report[1]). The small decrease in reflection with decreasing particle size noted in the opaque regions of the spectrum is produced in the theoretical treatment by the optical bonding effect which we referred to as the contact factor in our last report[1]. Hence it is clear that the theoretical model is entirely satisfactory for such smooth spherical particles. This evidence strongly suggests that our difficulties with quartz and corundum particles stem from the shapes of these particles or perhaps their state of aggregation. However, a few alternatives are conceivable such as the distinction between amorphous and crystalline materials and differences in packing density resulting from non spherical shapes.

If we assume that the difference in particle shapes is the correct explanation of the differing experimental results and that a dipole mechanism is essential to provide the additional absorption required, we are led to identify the dipoles with shape features such as edges, ridges, and other surface asperities. The scanning electron micrographs of 30μ and 120μ corundum particles shown in Figure 2 demonstrate

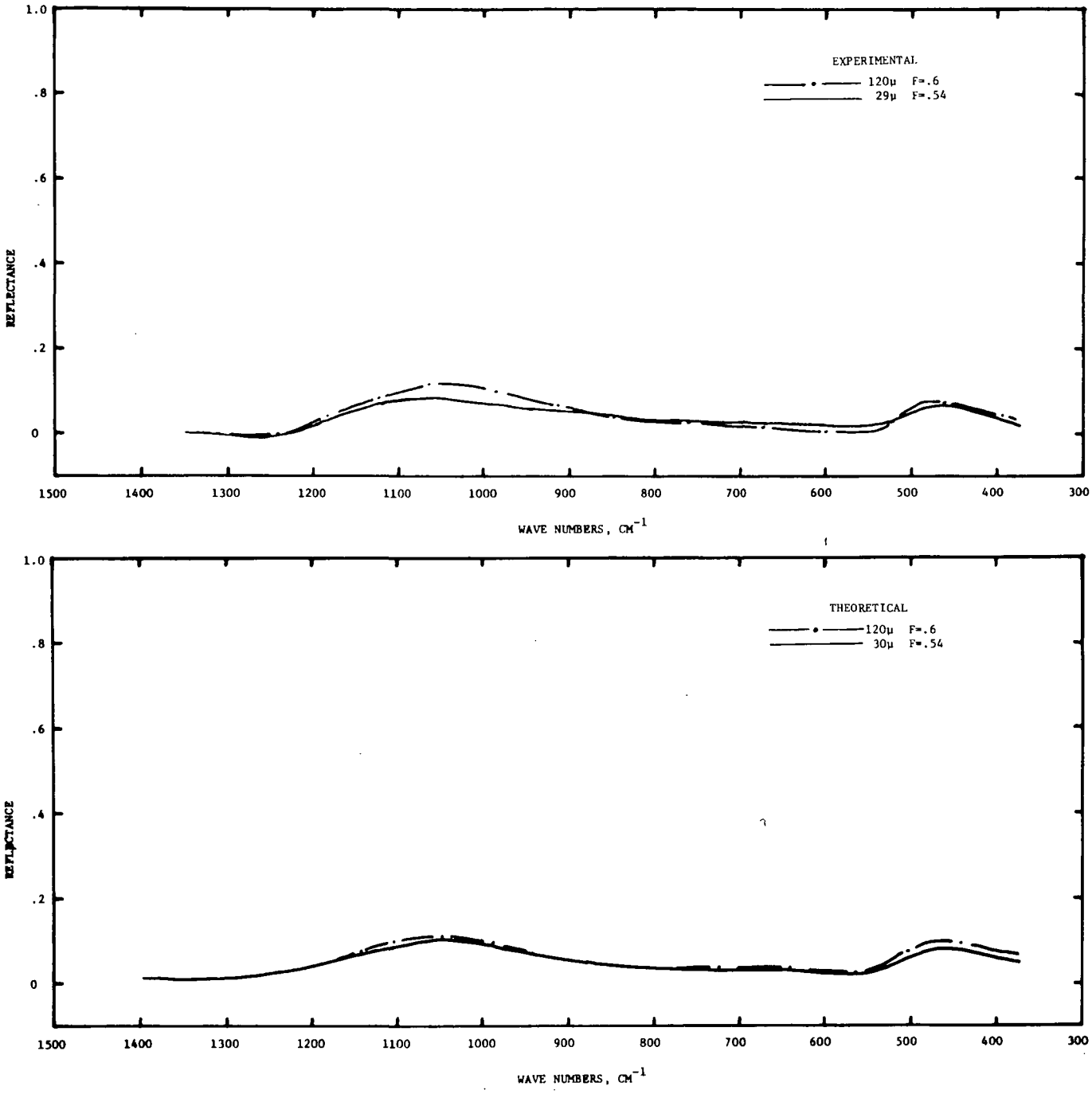


FIGURE 1 COMPARISON OF EXPERIMENTAL AND THEORETICAL REFLECTANCE OF GLASS BEADS

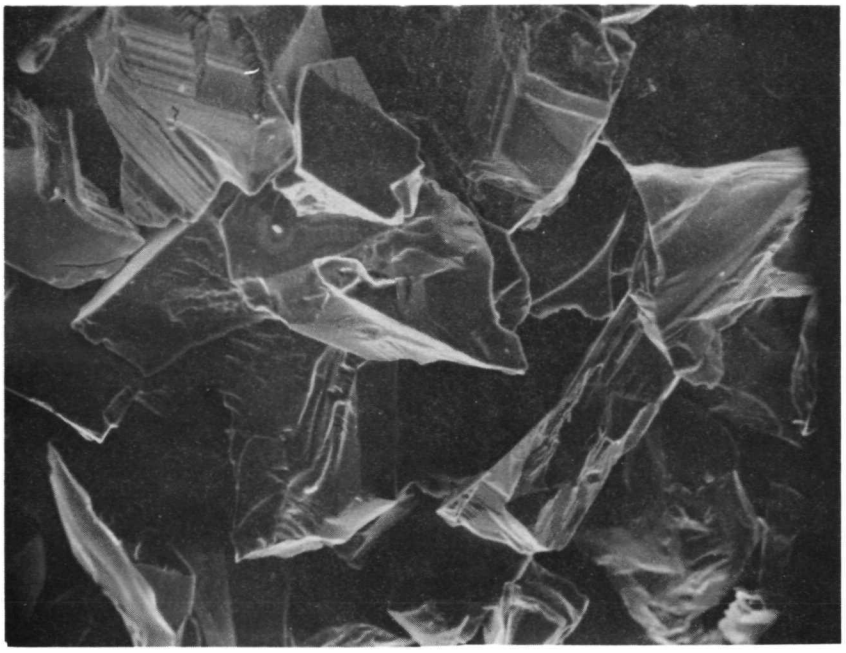

FIGURE 2a SCANNING ELECTRON MICROGRAPH OF STEPLIKE ASPERITIES

30μ CORUNDUM 1000X

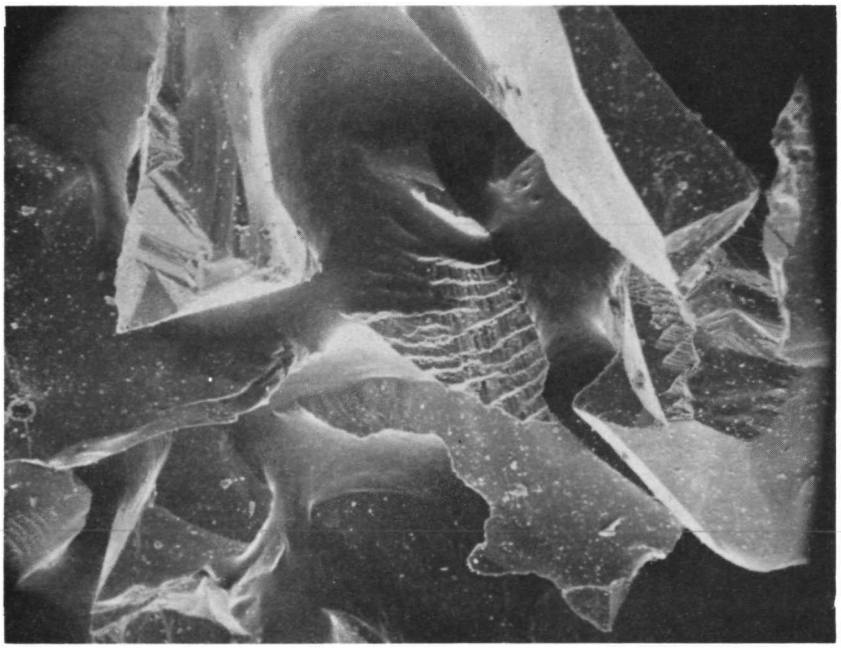

FIGURE 2b SCANNING ELECTRON MICROGRAPH OF STEPLIKE ASPERITIES AND ADDITIONAL FINES

120μ CORUNDUM 500X

that a hierarchy of steps or ridges are present on the surfaces of the particles in addition to the expected particle edges.

Such asperities provide a wave optical coupling mechanism whereby the external radiation can penetrate the particles more easily and so suffer increased absorption. The absorption cross-section of an elongated asperity such as an edge, ridge, or step is proportional to the length of the asperity.

This means that asperities distributed with constant surface density over the surfaces of the particles cause a loss in particle reflectance that is independent of particle size. The edges of the particles, on the other hand, cause a reflectance loss that varies inversely as the mean diameter of the particles, since the absorption cross-section of the edges is a larger fraction of the total surface area of a particle for small particles. Surface asperities should therefore be more important for large particles and edges more important for small particles.

## III. EVIDENCE FOR THE ROLE OF ASPERITIES

In this section we present the interlocking results of a number of experiments that lend additional strong support for the asperity hypothesis.

Figure 3 shows the reflectance spectrum of quartz powders of four different particle sizes. It is seen that in the regions of high particle opacity around 1150 $cm^{-1}$ and 500 $cm^{-1}$ there is a strong particle size effect corresponding to increasing absorption for the smaller particles, in agreement with edge-type absorption.

Figure 4 shows similar spectra of corundum powders. Again, the prominent particle size effect in the opaque regions at frequencies less than 900 $cm^{-1}$ can be attributed to edge absorption. The absorption in the region of the scallop from 860 $cm^{-1}$ to 660 $cm^{-1}$ includes a substantial component that is independent of particle size since even for 120μ particles the scallop is still quite significant and differs markedly from the single crystal spectrum in this region (see Figure 5). We attribute this absorption component to surface-distributed asperities.

Further evidence that the absorption in the scallop region of corundum contains a large contribution not caused by particle edges is given in Figure 5 which shows a comparison of the spectrum of a single crystal before and after abrading the surface of the crystal with 15μ diamond paste. It is seen that the surface asperities produced by roughening the surface cause a pronounced scallop. Figure 6 shows a stereo pair of scanning electron micrographs of a replica of the abraded surface. These photographs have been turned so as to produce the optical effect of the original surface rather than that of the replica. Abrasion can be seen to have produced a multitude of pits in the 2 - 10μ diameter range. The scallop feature shown in the spectrum was not reported in Barker's work[6] although he discussed

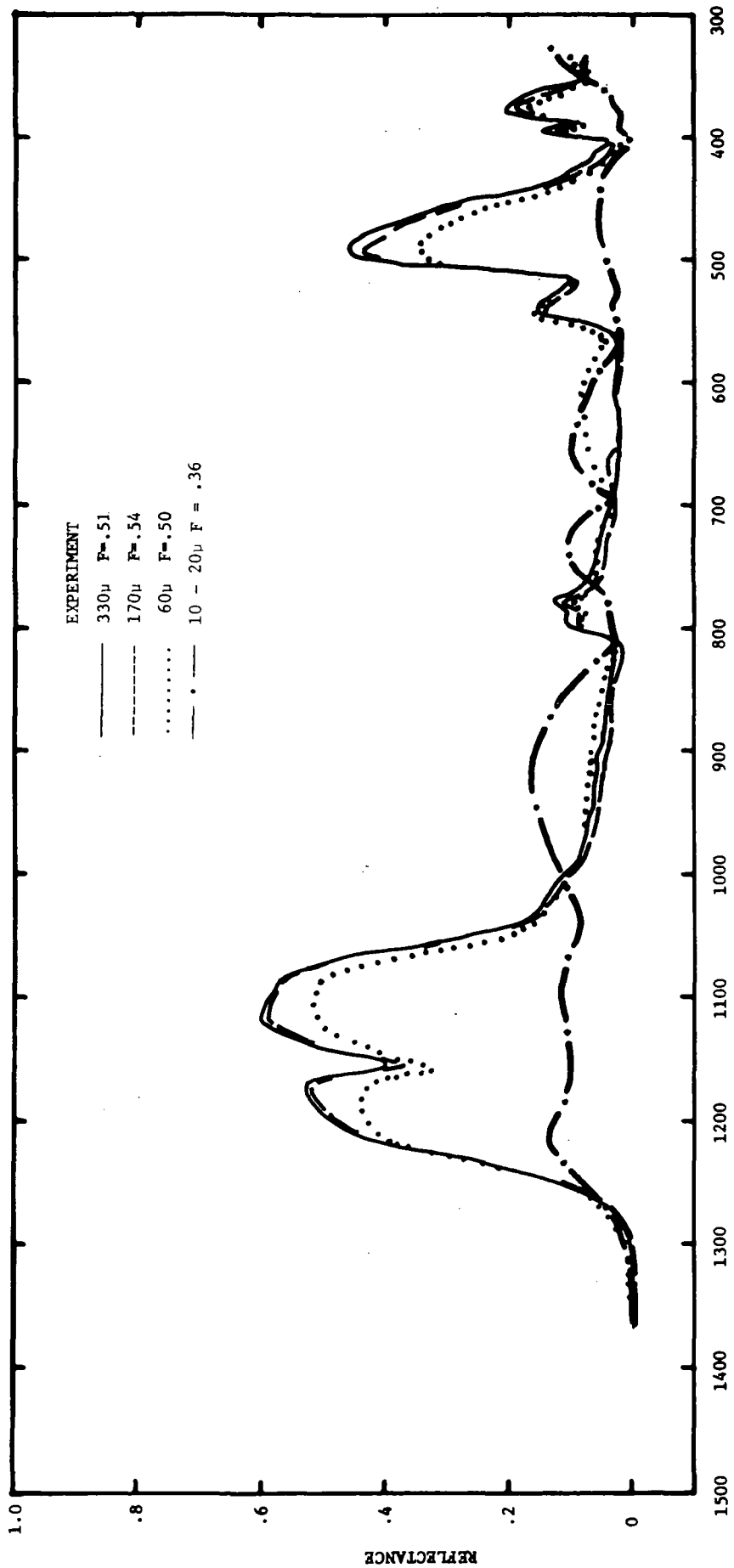


FIGURE 3 EXPERIMENTAL REFLECTANCE OF QUARTZ POWDERS

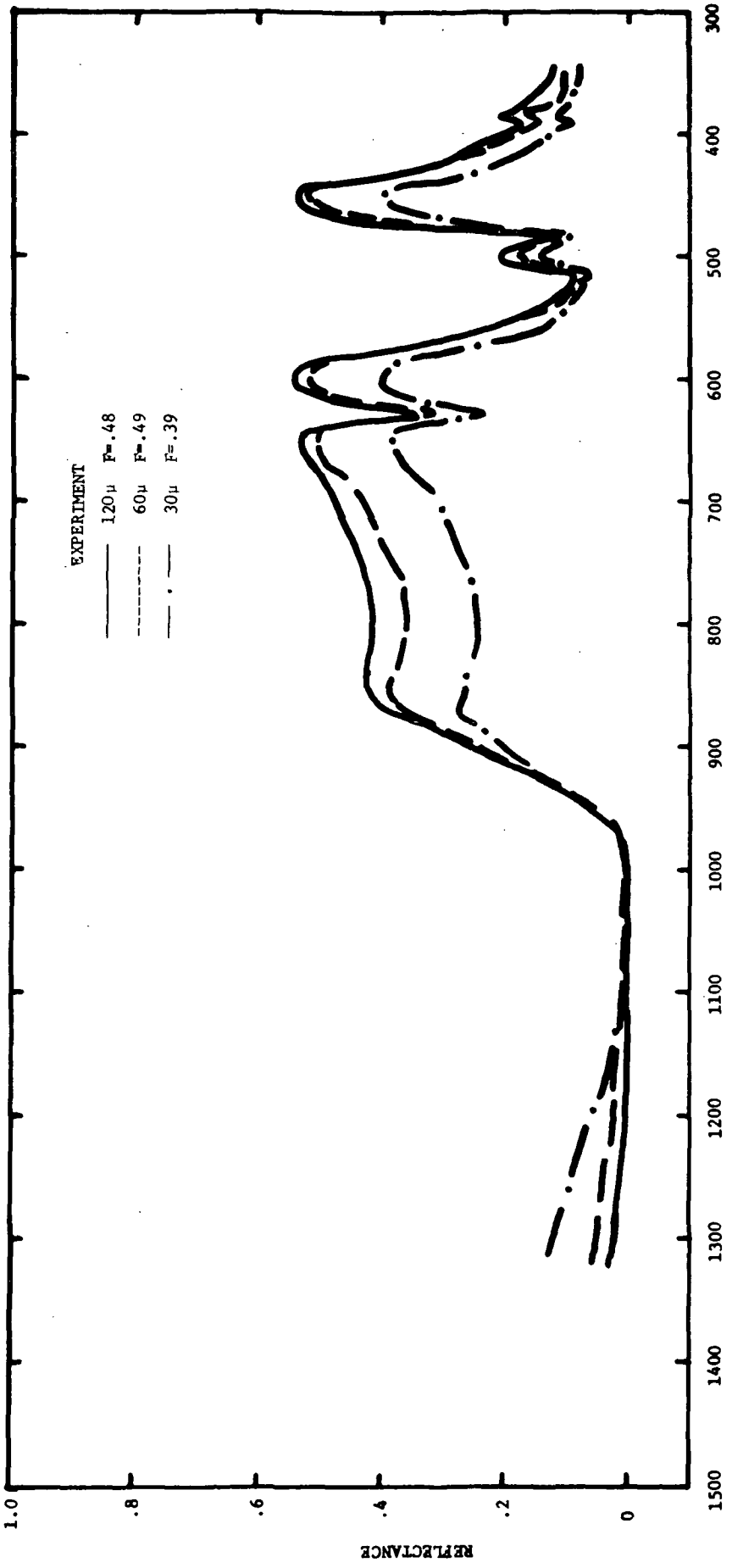


FIGURE 4 EXPERIMENTAL REFLECTANCE OF CORUNDUM POWDERS

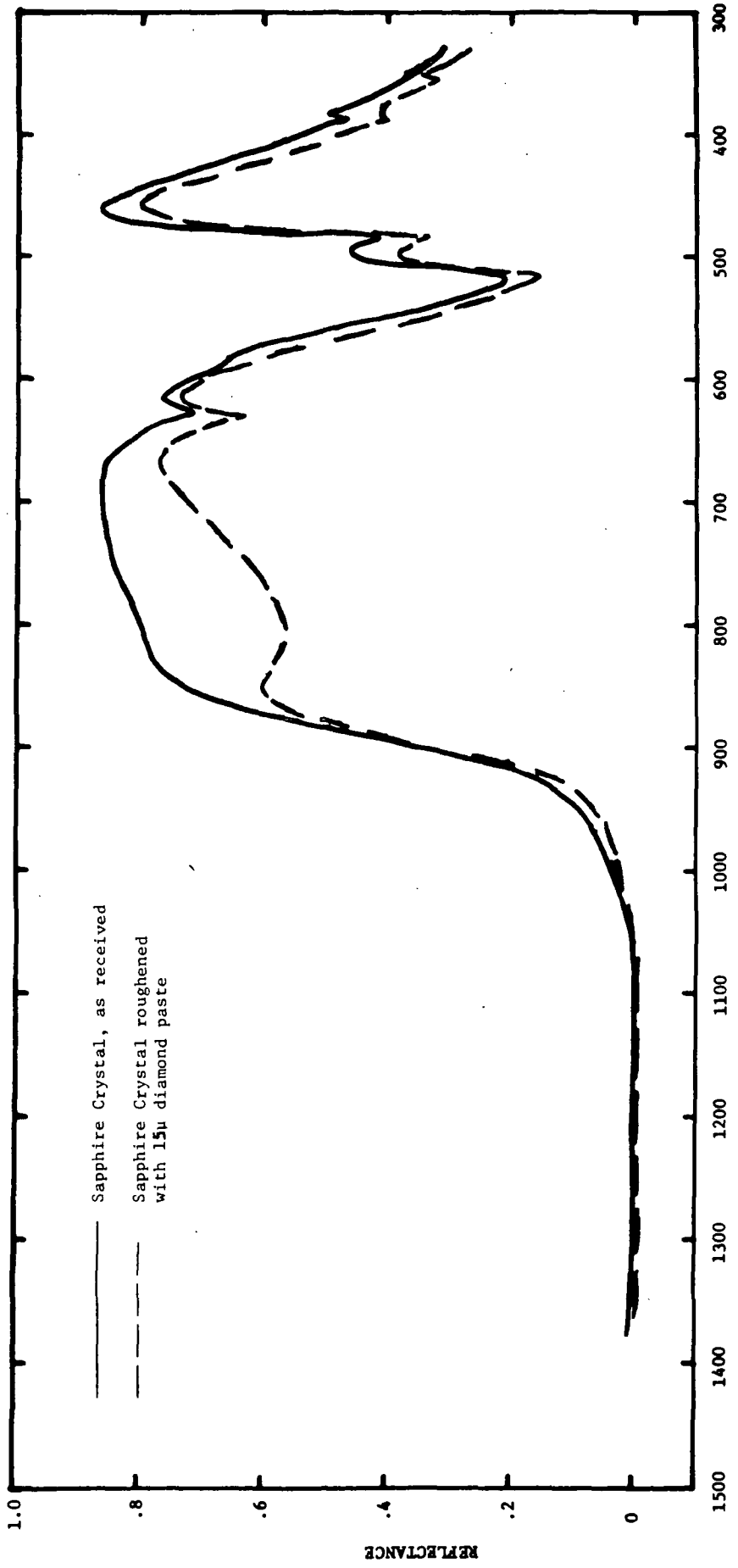


FIGURE 5 EXPERIMENTAL RESULTS OF ABRADING SAPPHIRE

other roughness dependent features at some length. We do not observe these other features. We carried out a second experiment along the same lines by abrading another sapphire sample with 6μ diamond paste. In this case, however, it was only possible to produce a series of scratches and the extensive pitting shown in Figure 6 did not occur. The spectrum produced by this treatment showed a very small scallop that did not warrant reproduction in Figure 5.

The conclusion that the scallop region of corundum involves surface asperities as well as edges is supported by the fact that quartz particles which for the most part have smoother surfaces (see Figure 11 of our last report[1]) give no scallop for large particle sizes. We attribute the onset of this type of feature at small particle sizes (see Figure 3) to the edges that become relatively more important for the small particles. It is important to note that quartz has similar optical constants in the relevant spectral region near 1100 $cm^{-1}$ to those for corundum in the scallop region. It is also worth noting that the scallop feature in small particle corundum is relatively independent of particle shape (also see Figure 18 of our previous report), i.e., the WCA powders were smooth platelets[7] (see Figures 7 and 8 of reference 8), while the present results are for the LWA material that has a chunky morphology. Some fines can be seen in the scanning electron micrographs. As surface asperities are not observed on the WCA corundum powders, we anticipate that such large smooth platelets should not show the scallop phenomenon. An excellent experimental test of the asperity concept will be provided by spectral measurements on smooth crystal spheres of corundum as neither edges nor surface asperities will occur. These are currently being prepared for us by the Manned Spacecraft Center of NASA.

It is perhaps worth mentioning that the spectrum of coarse quartz powder contaminated with a significant but small amount of fine quartz has a drastically reduced level in the opaque regions mentioned above (see Figure 13 of Reference 1). We interpret this

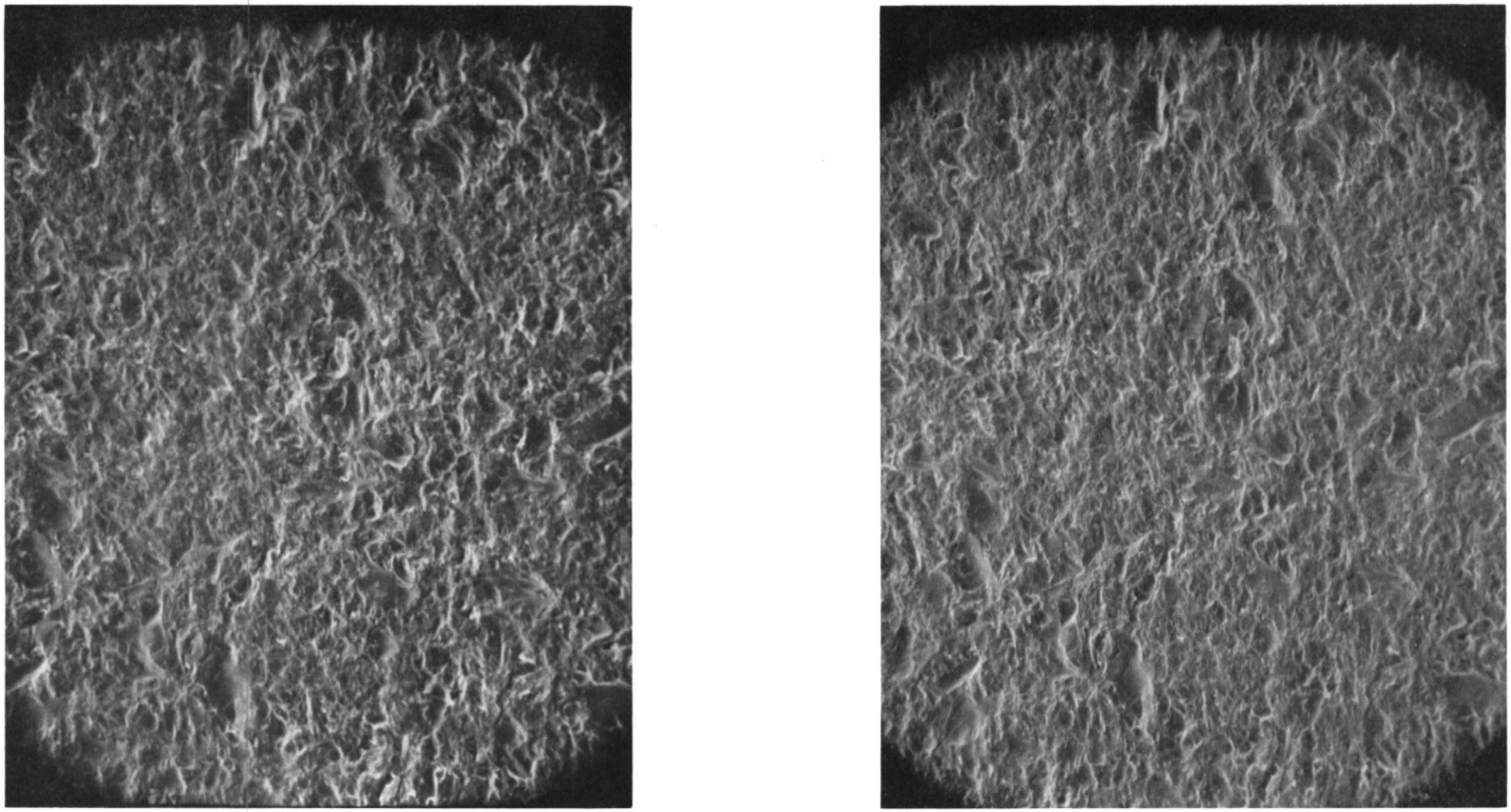

FIGURE 6 SCANNING ELECTRON MICROGRAPHS OF REPLICA OF ROUGHENED SAPPHIRE CRYSTAL

PHOTOGRAPHS ROTATED TO SIMULATE THE ACTUAL SURFACE (470X)

result as indicating that clinging fine particles are simply another form of asperities. The dipole hypothesis appears to be very attractive in light of the above discussion.

We will now consider the experimental evidence bearing on the aggregation hypothesis referred to in the introduction. Since the state of aggregation in the normal powder bed experiments is very difficult to establish using either optical or electron microscopy, we have carried out two types of experiments aimed at producing a high degree of uniformity in the packing density. If an aggregation effect is important in the powder bed experiments of Figure 4, then we expect to observe a significant reduction in the particle size effect in opaque regions for the less aggregated samples. We first attempted to investigate the hypothesis of an aggregation effect by examining the spectra of "monolayers" of corundum particles. These surfaces were prepared in a manner similar to that mentioned in our last report except that this time an attempt was made to completely cover the surface. The powder was again contacted with double faced masking tape and the excess shaken off. The process was repeated several times so as to provide a high degree of surface coverage in the monolayer. Scanning electron micrographs of the prepared surfaces are shown in Figure 7 with the scales arranged so as to provide comparable pictures. As can be seen, the coverage is quite high in both cases but somewhat less in the case of the 120μ particles. The spectra are shown in Figure 8. It is important to observe that the scallop phenomenon persists and that the general similarity of the spectra on the low frequency side of the Christiansen point at 1020 $cm^{-1}$ indicates that most of the spectral characteristics of the normal powder bed must therefore derive from the topmost layer of particles. Further, a particle size dependence in the opaque regions of the spectrum can still be seen even though the photographs do not indicate a significant difference in the degree of aggregation of the particles. However, a detailed comparison of the spectra of Figure 8 with those of Figure 4 indicates a diminution of the particle size effect. This might be

120μ CORUNDUM 50X

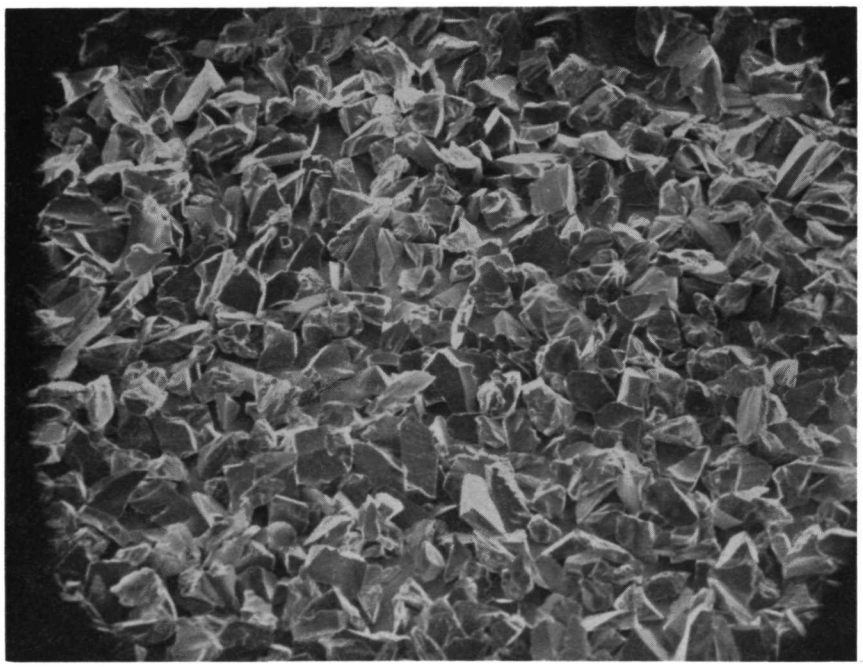

30μ CORUNDUM 200X

FIGURE 7 SCANNING ELECTRON MICROGRAPHS OF MONOLAYERS

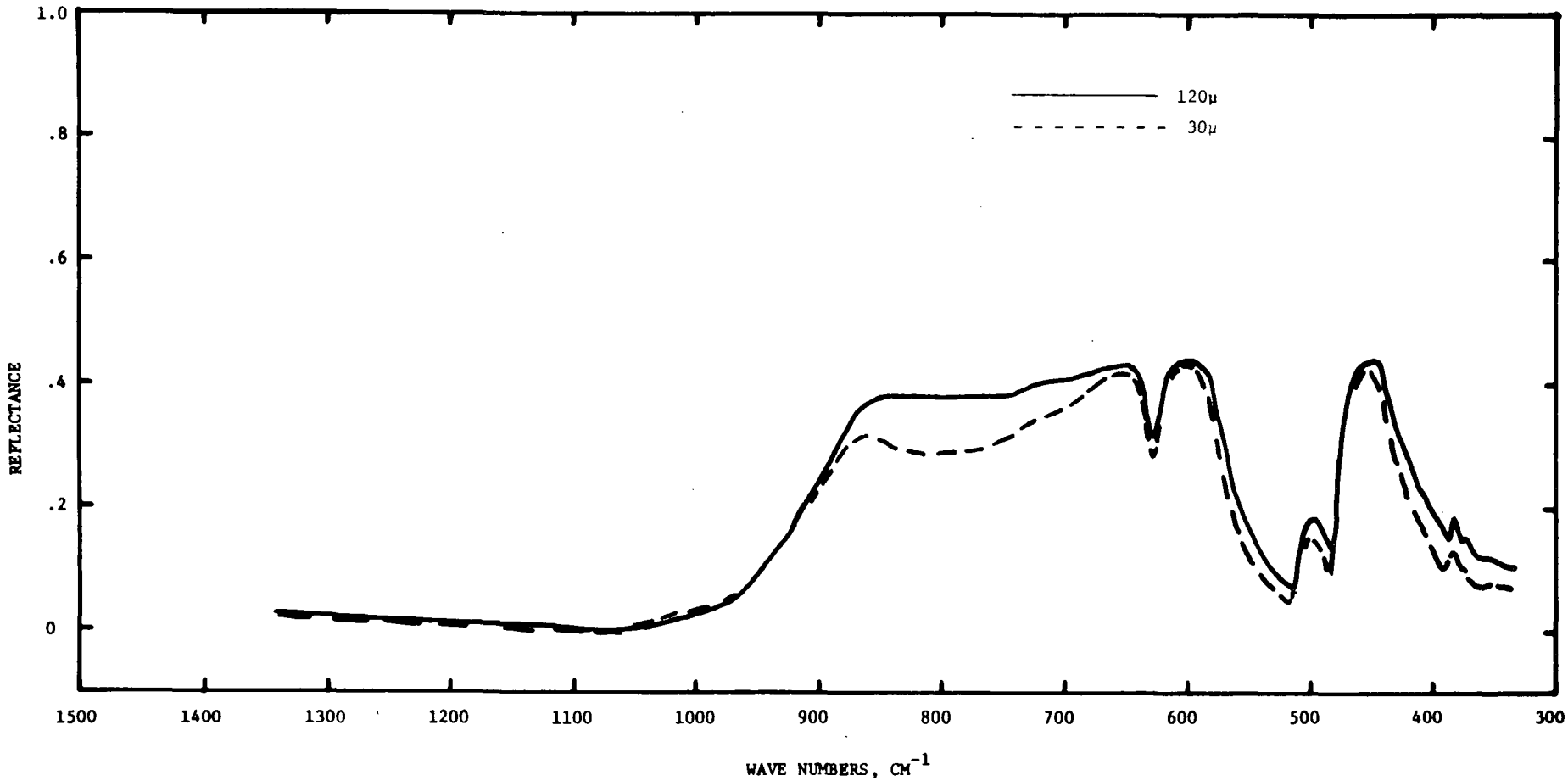


FIGURE 8 REFLECTANCE OF CORUNDUM MONOLAYERS

explained in terms of an aggregation effect in that the smaller particle size samples of Figure 4 might be somewhat aggregated. It is, however, quite plausible to explain the discrepancies between Figures 4 and 8 in terms of the surface coverages shown in the photographs of Figure 7. As stated above, the photograph of the 120μ corundum monolayer exhibits a noticeable area of incomplete coverage. In these regions the measured radiation pertains to the characteristics of the masking tape itself. The latter has been found to closely approximate a blackbody. Thus, assuming no significant temperature gradient between the tape and the monolayer particles, the exposed area of tape would result in a higher emittance (lowered reflectance). This is precisely the experimental result. The better coverage for the 30μ particles would reduce this effect, but despite this the reflectance can be seen to be reduced when compared to the 120μ monolayer data which argues for an asperity mechanism. Comparison with Figure 4 indicates a higher reflectance level for the 30μ monolayer. Reduced aggregation could be the cause but, as with the 120μ data, surface coverage can explain the effect. If we presume that the 30μ monolayer is more densely covered than the top layer in the 30μ powder bed and that some radiation originates in cavity-like areas of the powder bed, it is to be expected that the powder bed will appear blacker than the monolyer.

These speculations however are quite unsatisfactory and so another experiment was carried out to shed light on the problem. The same two grades of corundum were used and powder surfaces were prepared in a quite different manner. A suspension of the particles in methyl alcohol was decanted into a sample cup which had a hole in the bottom. The hole was covered with a fine mesh wire grid so as to prevent sample loss. Gentle aspiration was applied to the bottom of the container. While the wet powder was settling, a spatula was gently vibrated against the sample container. The spectral results of the samples prepared in this manner are shown in Figure 9. Again, a definite but reduced particle size effect can be seen. The density measurements shown in the figure (as volume fractions) indicated that

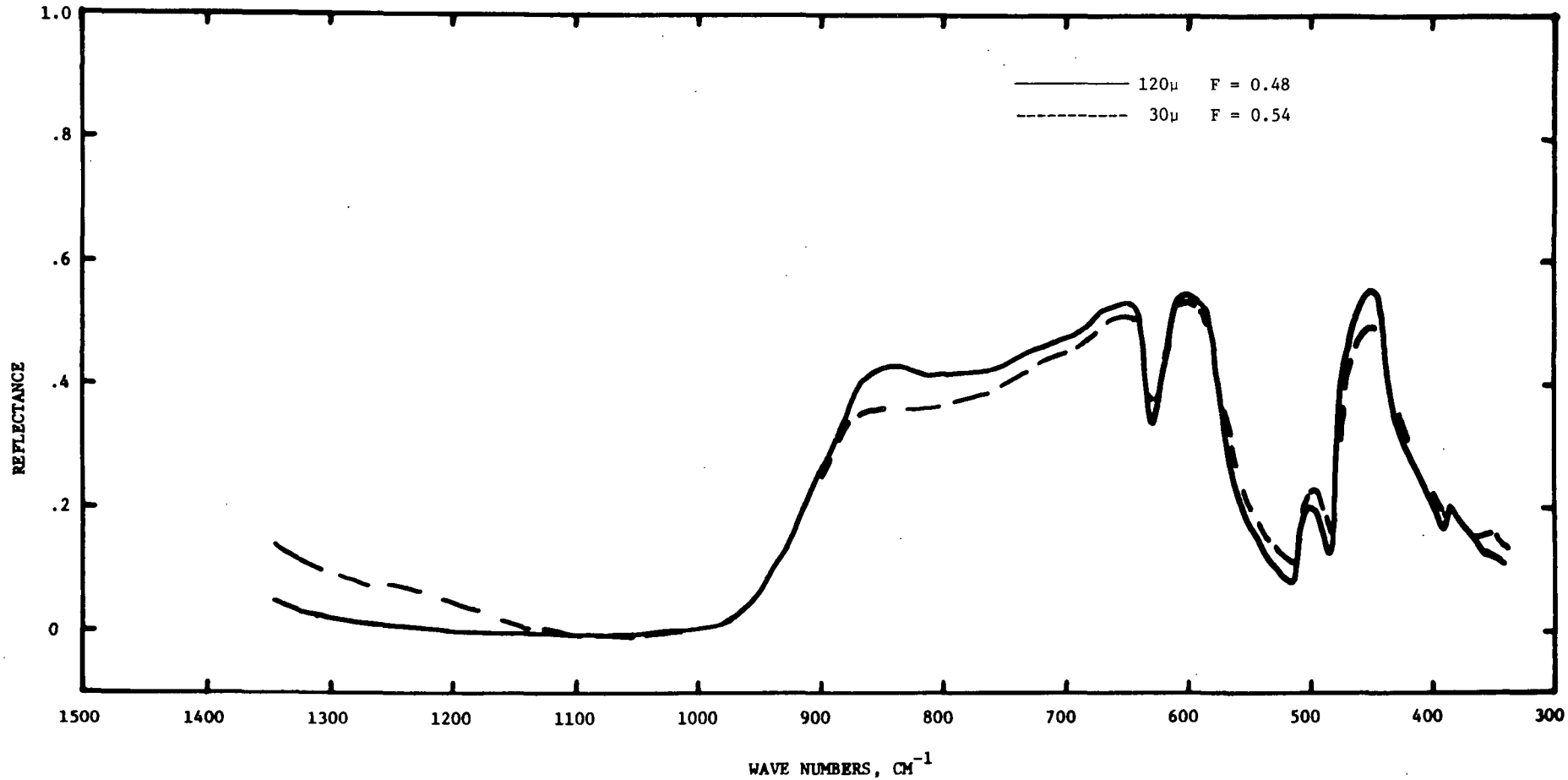


FIGURE 9 REFLECTANCE OF CORUNDUM POWDERS
(SURFACE PREPARED BY VIBRATION UNDER METHANOL)

the 120μ sample has undergone no change and indeed the 120μ sample produces an almost identical spectrum to that shown for the usual powder bed in Figure 4. This tends to confirm our explanation of the change for the 120μ monolayer sample. The 30μ powder spectrum shown in Figure 9, however, is considerably higher in reflectance than the comparable spectrum of Figure 4. However, it is to be noted that the shape of the scallop feature is noticeably different from that of the 30μ spectrum shown in either Figure 4 or Figure 8, particularly in the region near 860 $cm^{-1}$. Also the small feature near 500 $cm^{-1}$ lies above the comparable feature for the 120μ sample contrary to both the powder bed and monolayer experiments. These characteristics of the 30μ spectrum in Figure 9 suggest that there may have been a temperature error in the calibration of this spectrum. Such an error could have the effect of tilting the spectrum and therefore the experiment is inconclusive and must be repeated. However, the experiment did demonstrate that a significant compaction (and therefore possible reduction in aggregation) can be achieved for the smaller particles only. As the importance of an aggregation effect is still unproven we have included in our modified theory, as will be discussed later, only the effects of asperities and have postponed including aggregation effects.

## IV. FINE-PARTICLE EXPERIMENTS

At the time of our most recent previous report[1], the fine-particle model based on Rayleigh scattering by fluctuations in refractive index about a mean index determined by a Lorentz-Lorenz-like model, was found to be deficient in explaining the spectrum of 10-20μ quartz powder (see Figure 14 of that report). The real difficulty as mentioned in the introduction was that the theoretically predicted reflectance level was much too high. Two possible reasons for this level discrepancy are:

1. The particle size in the experiment is much too large for the concept of an average index to be valid.

2. Loss of reflection due to aggregation of the particles was not included in the theoretical treatment.

During the current report period we performed several experiments designed to examine these points. We first obtained from the Adolf Meller Co. a 0.3μ corundum powder (not the usual crystal structure for this particle size range). The powder was checked by X-ray techniques and proven to be corundum. The spectrum of a sample prepared in our usual manner is shown as the lowest curve in Figure 10. The broad feature in the usual reststrahlen region for corundum is small but observable and is an apparent continuation of the trends shown in Figure 4. The exceedingly small size of these particles relative to the wavelength of the radiation should permit the application of the Lorentz-Lorenz-like model. A theoretical spectrum using that model is the top curve shown in Figure 10 where $d_e$ refers to a correlation

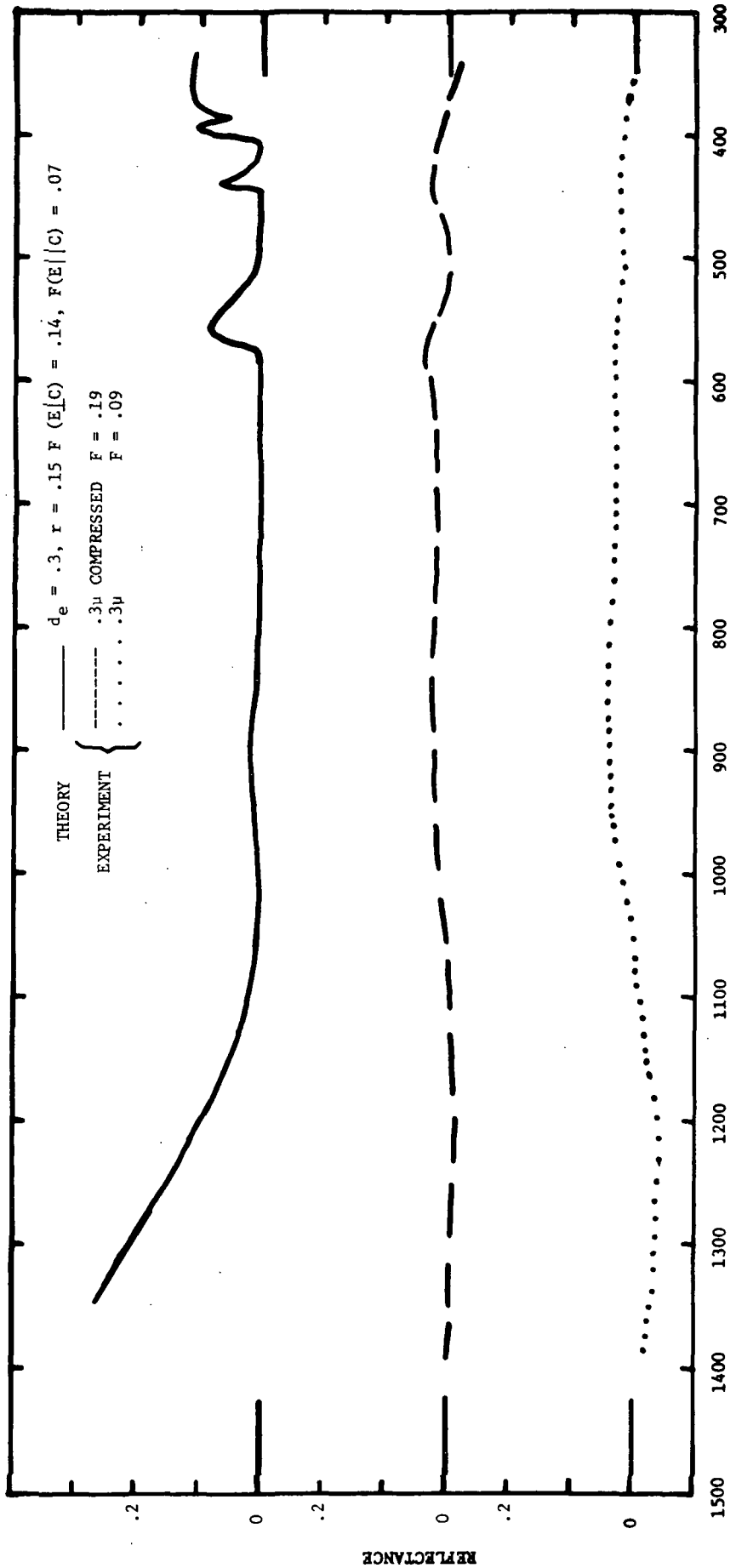


FIGURE 10 REFLECTANCE OF FINE CORUNDUM POWDER

distance and r refers to the radius of the particle. The treatment is that of our previous report, neglecting the Fresnel surface terms (either of the powder as a whole or of the individual clumps) on the assumption that the surfaces are likely to be sufficiently rough so that the radiation experiences no systematic discontinuity. This coupling mechanism is of the same nature as that invoked in the asperity hypothesis for coarse particles.

A comparison of the experimental and theoretical spectra indicates a great improvement in fit of the general level of the spectrum for these very fine particles, but the relatively strong features near 560 $cm^{-1}$ and 430 $cm^{-1}$, predicted by the theory, are scarcely visible experimentally. We concluded that the aggregation effect mentioned above might be the reason for this discrepancy. A second experiment was therefore carried out to test this idea. We gently compressed the 0.3μ corundum sample on the theory that the large cavities would be filled as the primary effect. The volume fraction of the powder was changed by the compression from $f = 0.09$ to $f = 0.19$. The spectral results of this experiment are also shown in Figure 10. Low frequency features similar to those predicted by the theory near 560 $cm^{-1}$ and 430 $cm^{-1}$ now show up more prominently. However, the predicted rise in reflectance at the high frequency end of the theoretical spectrum is not found in either experiment. This rise in the theoretical curve is the usual result of the small value of the absorption coefficient K, relative to the scattering coefficient, S in the relatively transparent spectral region involved. An additional absorption mechanism such as that produced by aggregation is required to reduce the theoretical curve. This hypothesis however leads to some difficulties with respect to the low frequency end of the spectrum which may require a reconsideration of the possibility of Fresnel reflection. The latter is suggested by the low flat level of the high frequency data. Further work is required in this area.

The experimental curves in Figure 10 have been normalized by our usual technique employing the Christiansen frequency[7,3]. In this case

the apparent reduction in overall level of the compressed powder with respect to the low density sample may be an artifact resulting from two effects. First, small temperature errors have a disproportionately large effect when a detailed comparison of two curves is involved. The second effect involves the use of the Christiansen effect in the presence of the significant temperature gradient resulting from the fluffy nature of the fine-particle powder bed. The problem of the use of the Christiansen technique in the presence of significant temperature gradients will be discussed below.

## V. THEORETICAL DEVELOPMENTS

During the present report period we have made a number of significant improvements in the theory. These include the wave theory corrections mentioned earlier for the effect of edges and other asperities, and geometrical optics modifications of the scattering and absorption cross-sections involving a more accurate angular distribution function.

### A. EFFECT OF EDGES

In the reststrahlen regions of the spectrum a mineral particle with a smooth surface has a high Fresnel reflectance. The reflectance is, however, considerably reduced if the particle has sharp edges and other sharp asperities such as ridges, steps, etc. The distribution of asperities acts as a graded transition layer between the vacuum and the interior of the particle. The degree of matching from the vacuum to the particle refractive index depends on the structure of the asperities (i.e., the effective thickness of the transition layer) relative to the wavelength. In the case of edges we assume that the effective depth of the asperity is comparable with the skin depth $\delta$ of penetration of the radiation. The effective width, b, is assumed to be some fraction of a Fresnel zone, say $b = \lambda_o/2\pi$. The length of the asperity is of the order of the particle size d. We further assume that the absorption cross-section of an edge may be calculated by treating the edge as though it were an isolated ellipsoidal particle with dimensions $\delta$, b, d.

The dipole moment $\vec{\mu}$ induced in an ellipsoidal particle by a static electric field $\vec{E}$ has the components

$$\mu_x = \frac{\chi V}{1 + L\chi} E_x \qquad (1)$$

$$\mu_y = \frac{\chi V}{1 + M\chi} E_y \tag{2}$$

$$\mu_z = \frac{\chi V}{1 + N\chi} E_z \tag{3}$$

where $V$ is the volume of the particle, $\chi = (K - 1)4\pi$ is the electric susceptibility of the material of the particle, and L, M, N are the depolarization factors which depend on the shape of the ellipsoid. Here $K$ is the dielectric constant of the particle material. The axes x, y, z are aligned with the principal axes of the ellipsoid.

We assume that the ellipsoid is small enough so that the amplitude of the oscillating dipole moment induced by an infrared wave has approximately the static value given by (1) - (3). In terms of the complex refractive index of the ellipsoid the susceptibility takes the form

$$\chi = (m^2 - 1)/4\pi \tag{4}$$

The power absorbed by the ellipsoid is given by the expression

$$W = \frac{1}{2} \text{Re} \left(\vec{E}^* \cdot \frac{d\vec{\mu}}{dt}\right)$$

$$= -\frac{\omega}{2} \text{Im} \left(E_x^* \mu_x + E_y^* \mu_y + E_z^* \mu_z\right) \tag{5}$$

where $\omega$ is the angular frequency of the electric field.

From (1) - (4), (5) becomes

$$W = -\frac{\omega V}{8\pi} \text{Im} \left(m^2 - 1\right) \left\{ \frac{|E_x^2|}{1 + \frac{L}{4\pi}(m^2-1)} + \frac{|E_y^2|}{1 + \frac{M}{4\pi}(m^2-1)} + \frac{|E_z^2|}{1 + \frac{N}{4\pi}(m^2-1)} \right\} \tag{6}$$

For the case of diffuse incident radiation we average $W$ over all inclinations of the electric field relative to the axes of the ellipsoid. The result is

$$\overline{W} = -\frac{\omega V|E|^2}{24\pi} \mathrm{Im}(m^2-1) \left\{ \frac{1}{1+\frac{L}{4\pi}(m^2-1)} + \frac{1}{1+\frac{M}{4\pi}(m^2-1)} + \frac{1}{1+\frac{N}{4\pi}(m^2-1)} \right\} \quad (7)$$

where $E$ is the amplitude of the incident radiation.

Since the edges of particles vary in sharpness, that is in the angle between the two adjacent facets, we now average (7) with respect to the cross-sectional shape of the ellipsoid. For this purpose we assume that the length $d$ of the ellipsoid is large compared with $\delta$ or $b$. In that case $N = 0$ and $L + M = 4\pi$. Therefore (7) can be expressed in terms of $L$ alone. For simplicity, we assume that the variation in edge sharpness is such that all values of $L$ from 0 to $4\pi$ occur with equal probability. Then the averaging over L can be done easily and gives the result

$$\overline{\overline{W}} = -\frac{\omega V|E|^2}{24\pi} \mathrm{Im}\,(m^2 - 1 + 4 \log m)$$

$$= -\frac{\omega V|E|^2}{24\pi} \left\{ \mathrm{Im}\,(m^2) + 4\,\mathrm{Arg}\,m \right\} \quad (8)$$

where Arg denotes argument and Im denotes imaginary part of a complex number.

The total diffuse radiation power incident on a cube-shaped particle of edge $d$ is

$$W_i = \frac{c|E|^2}{24\pi} \cdot 6d^2 \quad (9)$$

where $c$ is the speed of light. Therefore the ratio of the power

absorbed by the 12 edges to the total incident power is, from (8) and (9),

$$\frac{W_e}{W_i} = -\frac{4\pi}{\lambda_o}\frac{b\delta}{d}\left\{\text{Im}\ (m^2) + 4\ \text{Arg}\ m\right\} \tag{10}$$

where $\lambda_o = 2\pi c/\omega$ is the free-space wavelength of the radiation and $V = b\ \delta\ d$. It is to be noted that the fractional power loss due to the edges is proportional to $1/d$ which agrees with the observed trend of the reflectance with particle size.

The average diffuse reflectance $R_o'$ of the particle surface, allowing for the edge effect, is

$$R_o' = R_o\ (1 - \frac{W_e}{W_i}) \tag{11}$$

where $R_o$ is the uncorrected reflectance. This expression is not valid when $W_e > W_i$, which occurs when the particle is so small that the edge regions cover the whole surface of the particle. To avoid this difficulty we write (11) in the form

$$R_o' = R_o\ e^{-W_e/W_i} \tag{12}$$

which reduces to (11) when $W_e/W_i << 1$.

In expression (10) for $W_e/W_i$ the quantity $\delta$ is the mean depth below the surface at which the Poynting's vector has fallen to $1/e$ of its value at the surface. For the case of a wave incident at an angle $\theta$ the penetration depth is

$$\delta\ (\theta) = \frac{\lambda_o}{4\pi\ \text{Re}\ \sqrt{\sin^2\theta - m^2}} \tag{13}$$

Since $\delta(\theta)$ tends to infinity in the case of transparent ($k = 0$) particles when $\sin\theta$ is less than $n$ we again use the exponential approximation and write (13) as

$$\delta(\theta) = \frac{\lambda_o}{4\pi}\left(1 - e^{-\frac{1}{\mathrm{Re}\sqrt{\sin^2\theta - m^2}}}\right) \qquad (14)$$

We could obtain the average value $\delta$ by integrating (14) over all values of $\theta$ from 0 to 90° with a weighting factor $\cos\theta$ to allow for diffuse incident radiation. However, to avoid this integration step in the computer we actually replace $\theta$ by its mean value of 45° and so obtain

$$\delta = \frac{\lambda_o}{4\pi}\left(1 - e^{-\frac{1}{\mathrm{Re}\sqrt{0.5 - m^2}}}\right) \qquad (15)$$

The error involved in this simplification is expected to be very small.

By trial we have found that a value of the transverse dimension b of $\lambda_o/2\pi$ gives good agreement with experiment. Therefore (12) becomes after substitution from (10) and (15):

$$R_o' = R_o\, e^{\frac{\lambda_o}{2\pi d}\left\{\mathrm{Im}(m^2) + 4\,\mathrm{Arg}\,m\right\}\left(1 - e^{-\frac{1}{\mathrm{Re}\sqrt{0.5 - m^2}}}\right)} \qquad (16)$$

## B. EFFECT OF SURFACE ASPERITIES

Surface asperities such as steps, ridges and bumps also cause extra absorption which can be attributed, as with edges, to the effect of induced dipoles. Since the asperities do not in general have one dimension that is much larger than the other two we now consider the asperities as ellipsoids of revolution of volume $V$ characterized by the depolarization factors L, M, N which have the values L, L, $4\pi - 2L$ respectively, where L varies from 0 to $2\pi$.

On substituting for M and N into (7) and averaging over L we find for the average power absorbed per dipole

$$\overline{\overline{W}} = -\frac{\omega V|E|^2}{24\pi}\left\{2 \text{ Arg } m + 4 \text{ Arg } (m^2 + 1)\right\} \qquad (17)$$

Let N be the average number of asperities per unit area of particle surface. Then in place of (10) we find for the ratio of power $W_a$ absorbed by asperities to the total incident power $W_i$,

$$\frac{W_a}{W_i} = \frac{2\pi N V}{\lambda_o}\left\{-2 \text{ Arg } m - 4 \text{ Arg } (m^2 + 1)\right\} \qquad (18)$$

Thus the change in reflectance due to the surface asperities is independent of particle size provided that N and V are independent of d. Therefore under these conditions surface asperities do not contribute to the observed particle size effect.

Figure 11 shows a comparison of the average power $\overline{\overline{W}}$ absorbed by an edge (Eq 8), and that absorbed by a surface asperity (Eq 17), for the scallop region of corundum. It is seen that each effect produces an absorption maximum in this region. Either mechanism could therefore be used to explain the scallop. The experiment with the abraded single crystal, discussed earlier, shows however, that the scallop can be made to appear with only surface distributed asperities. On the other hand, the particle size dependence seems to require the edge effect. It therefore appears likely that both types of asperity contribute significantly to extra absorption by the particles. At present we have included only the edge effect in our computer program.

It is worth noting that in order to obtain good agreement between theory and experiment in the scallop region it is necessary to average over a wide range of asperity shapes as described above. A single shape produces sharp resonance-like features which arise when m is close to the poles associated with the denominators in Eq (7). The phenomenon appears to be characteristic of dipoles induced in small

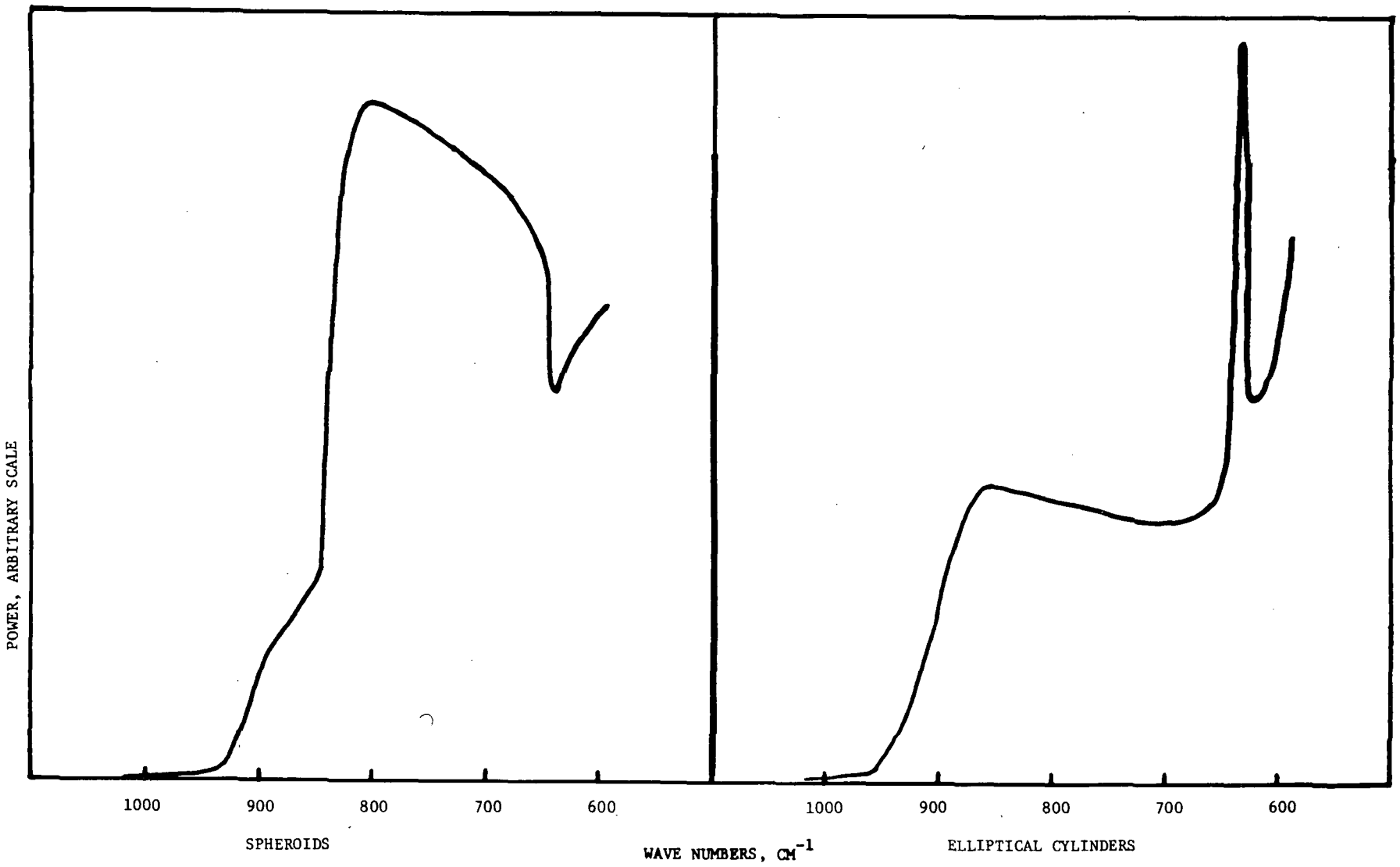


FIGURE 11 POWER ABSORBED DUE TO INDUCED DIPOLES FOR CORUNDUM

particles in reststrahlen bands where the complex index of refraction has wide excursions in the complex plane as a function of wavelength*. We have noticed similar troublesome resonance behavior in the Lorentz-Lorenz theory for very small particles which also act as dipoles. It is therefore likely that our fine particle theory would be considerably improved if we were to average over a range of particle shapes.

## C. SINUSOIDAL GRATING MODEL

As an alternative to the dipole model for surface asperities described above, we have attempted to explain the results of the abraded single crystal in terms of a single crystal with a sinusoidal surface of periodicity less than the wavelength of the radiation. A plane wave incident at some angle $\theta_o$ on such a grating produces only a zero-order reflection spectrum at large distances from the grating since the grating formula $\sin\theta - \sin\theta_o = n\lambda/D$ can only be satisfied for $n = 0$ when $\lambda/D$ is greater than unity.

Close to the surface of the grating, however, a large number of higher order reflection spectra exist in the form of non-radiating evanescent waves. Below the surface there is an array of transmitted orders most of which are approximately evanescent in nature if the absorption index is small.

If we consider only the $N$ lowest order reflected beams and the same number of transmitted beams we can obtain a solution that exactly satisfies the boundary conditions on the surface at $2N$ evenly spaced

---

* In this regard we wish to withdraw Eq (43) of our last report[1] because of an algebraic error which made it appear that dipoles induced in particles of uniform size and shape could explain the scallop effect. When corrected, the equation no longer gives the scallop.

points within each period of the sinusoidal surface. The 2N simultaneous equations in the amplitudes of the various orders can then be solved by a computer for the zero-order reflected beam. We discovered, however, that the computed reflectance converges very slowly as a function of N so that no useful result has been obtained to date. Further study of the problem is desirable since a solution would provide a valuable check on our dipole model for asperities.

## D. IMPROVEMENT IN THE ANGULAR DISTRIBUTION IN THE COARSE PARTICLE THEORY

In our original coarse particle theory based on the random interface model, in order to obtain a closed form solution for the refractive part of the scattering cross-section, we assumed that the refracted rays produced by a randomly oriented interface were uniformly distributed within a cone. We have now removed this assumption and at the same time have allowed for correlation in the orientation of successive interfaces.

In the revised calculation we return to a particle model in place of the interface model and for simplicity (in this part of the theory) treat the particles as spheres of radius a. We consider a parallel bundle of rays to be incident on one of the spheres as in Figure 12. For a ray with incident angle $\theta$, refraction angle $\psi$, (taken to define the direction of Poynting's vector) deviation angle $\phi$, and transmission distance $\ell$ we have the following relations.

$$\phi = 2|\theta - \psi| \tag{19}$$

$$\tan \psi = \frac{\sin \theta}{\mathrm{Re}\ \sqrt{m^2 - \sin^2\theta}} \tag{20}$$

$$\ell = 2\, a \cos\psi \tag{21}$$

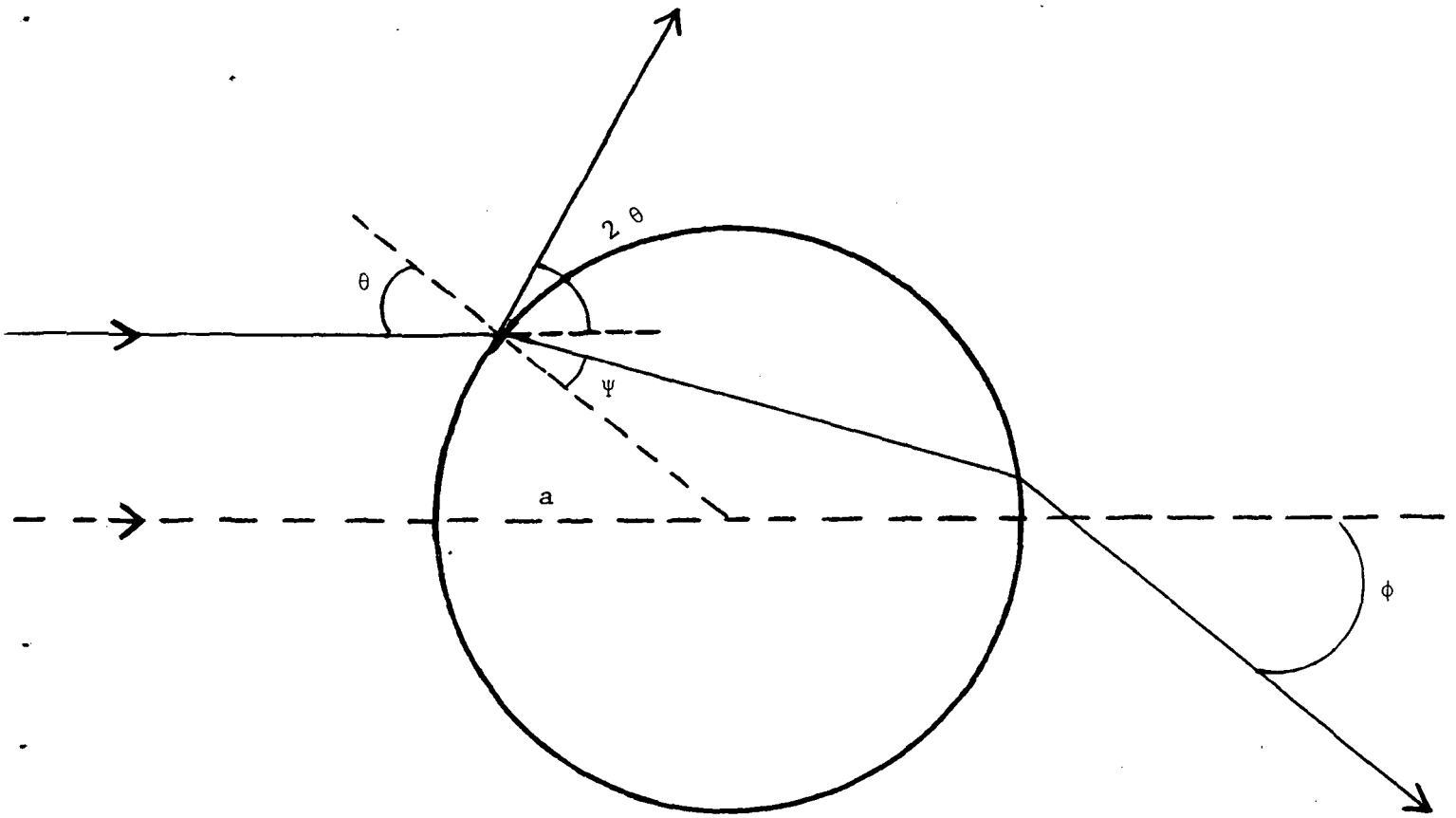


FIGURE 12 DIAGRAM OF REFLECTION AND REFRACTION BY A SPHERE

The angle $\psi$ given by (20) is the angle of the Poynting's vector in the sphere relative to the radius vector to the point of entry of the ray. Eq (20) reduces to the ordinary law of refraction when $m$ is real.

The cross-section for transverse scattering by direct refraction is given by the expression

$$(\sigma_t')\ \text{refraction} = \pi a^2 \int_o^{\pi/2} (1 - R_o)^2\ T \sin^2\phi \sin 2\theta d\theta \qquad (22)$$

where

$$R_o = \frac{1}{2} (R_{||} + R_{\perp}) \qquad (23)$$

is the Fresnel reflectance for unpolarized radiation at the angle $\theta$, and

$$T = e^{-\frac{4\pi R\ell}{\lambda_o}} \qquad (24)$$

is the transmission factor due to absorption in the sphere.

The factor $(1 - R_o)^2$ allows for the reflection loss at the two interfaces. The term $\sin 2\theta d\theta$ gives the incident power distribution over the illuminated hemisphere. The factor $\sin^2\phi$ is an assumed weighting factor which is maximum for rays that emerge transversely and zero for rays that emerge directly forward or directly backward. The integration over $\theta$ from 0 to $\pi/2$ covers all incident rays. The prime on $\sigma_t'$ indicates that the cross-section refers to collimated rather than diffuse incident radiation.

In like manner, the cross-section for back scattering by direct refraction is

$$(\sigma_b')_{\text{refraction}} = \pi a^2 \int_{\phi > \frac{\pi}{2}} (1 - R_o)^2\ T \cos^2\phi \sin 2\theta\ d\theta \qquad (25)$$

where the weighting factor $\cos^2\phi$ peaks in the backwards direction ($\phi = \pi$) and is zero in the transverse direction ($\phi = \pi/2$). The range of integration in $\theta$ is such as to include all emergent rays, if any, for which $\phi \geqq \pi/2$. The limits for $\theta$ are determined by computing $\phi$ from (19) and (20) as a function of $\theta$.

The cross sections for externally reflected radiation are

$$(\sigma_t')_{\text{reflection}} = \pi a^2 \int_0^{\pi/2} R_o \sin^2 2\theta \sin 2\theta \, d\theta \tag{26}$$

$$(\sigma_b')_{\text{reflection}} = \pi a^2 \int^{\pi/4} R_o \cos^2 2\theta \sin 2\theta \, d\theta \tag{27}$$

since the deflection $\phi$ is $2\theta$ in this case.

We obtain the cross-section for diffuse incident radiation by Conel's method[3] of regarding the diffuse radiation as consisting of six mutually perpendicular beams, inclined at an angle of $\cos^{-1}(1/\sqrt{3})$ to the axis of symmetry, with three of the beams pointing forwards and three backwards. It then follows that the diffuse backscattering cross-section $\sigma_s$ is related to the collimated beam cross-sections $\sigma_b'$ and $\sigma_t'$ by the formula

$$\sigma_s = \sigma_b' + \frac{1}{2}\sigma_t' \tag{28}$$

Therefore,

$$(\sigma_s)_{\text{refraction}} = (\sigma_b')_{\text{refraction}} + \frac{1}{2}(\sigma_t')_{\text{refraction}} \tag{29}$$

$$(\sigma_s)_{\text{reflection}} = (\sigma_b')_{\text{reflection}} + \frac{1}{2}(\sigma_t')_{\text{reflection}} \tag{30}$$

A final contribution to the scattering cross-section comes from radiation that suffers one or more internal reflections. For a given angle of incidence the total fractional amount of such radiation is easily shown to be $R_o (1 - R_o)^2 T^2/(1 - R_o T)$. Since the emerging rays included in this total are widely distributed over the sphere, we assume for simplicity that the angular distribution is approximately uniform. Therefore, one-half of this radiation is backscattered and the diffuse backscattering cross-section is

$$(\sigma_s)_{\text{internal reflection}} = \frac{1}{2}\pi a^2 \int_o^{\pi/2} \frac{R_o(1 - R_o)^2 T^2}{1 - R_o T} \sin 2\theta \, d\theta \qquad (31)$$

The total diffuse backscattering cross-section is

$$\sigma_s = (\sigma_s)_{\text{refraction}} + (\sigma_s)_{\text{reflection}} + (\sigma_s)_{\text{internal reflection}} \qquad (32)$$

The backscattering coefficient $S$ is then obtained from the formula

$$S = \sqrt{3}\, N\, \sigma_s \qquad (33)$$

where N is the number of particles per unit volume given in terms of the volume fraction $f$ and the particle radius $a$ by the relation

$$N = \frac{3f}{4\pi a^3} \qquad (34)$$

The factor $\sqrt{3}$ arises from the obliquity of the beams in the six-beam model.

The spherical particle model has been used only to provide a better angular distribution from which better values for the scattering and absorption can be derived. In the overall coarse particle theory we allow for the effects of edges by replacing $R_o$ in the foregoing equations by $R_o'$ defined by Eq. (16). Allowance for contacts between particles is made as before by a correction to the scattering coefficient S.

We obtain the absorption cross-section of the particle by first calculating the fractional absorption for a given incident ray which is readily found to be $(1 - R_o)\ (1 - T)\ /\ (1 - R_oT)$. Therefore the absorption cross-section is

$$\sigma_a = \pi a^2 \int_o^{\pi/2} \frac{(1- R_o)\ (1 - T)}{1 - R_oT} \sin 2\theta\ d\theta \qquad (35)$$

The diffuse absorption coefficient is then obtained from the formula

$$K = \sqrt{3}\ N\ \sigma_a$$

## VI. COMPARISON OF THEORY WITH EXPERIMENT

### A. SINGLE MINERALS

The most important change made in the coarse particle model during the present report period has been the inclusion of the wave optical effect of the particle edges as discussed in the previous section. A comparison of the theoretical spectra with experimental data for corundum is shown in Figure 13. As can be seen the proper particle size trends and general spectral levels are well represented by the present model. It is to be noted that the theory correctly predicts the opposite trends observed in the data for the opaque regions at frequencies less than 925 $cm^{-1}$ and the transparent region at higher frequencies. In addition, the scallop phenomenon is in reasonable agreement with the experimental data. We believe that this agreement will be enhanced when we include the effect of the surface asperities known to be present in corundum (Figure 2). The reason is apparent from the relative absorption effects of edges and asperities shown in Figure 11.

Figure 14 shows a similar comparison for quartz powders. In this figure the opaque and transparent spectral regions again show opposite particle size trends that are well predicted by the theory. We have used the coarse particle theory in this case over a much larger range of particle sizes than in the case of corundum. In particular, we note that particle sizes as low as 10μ - 20μ are qualitatively fitted by the theory. A feature similar to the scallop shown for corundum begins to be observed both in experiment and theory in the 1100 $cm^{-1}$ to 1200 $cm^{-1}$ region for the small particle size quartz. This is a spectral region of similar optical constants to those for the scallop region in corundum. We attribute the less prominent scallop in quartz powders in part to the relative absence of surface asperities (compare Figure 2 with Figure 11 of our last report[1]). The theoretical results

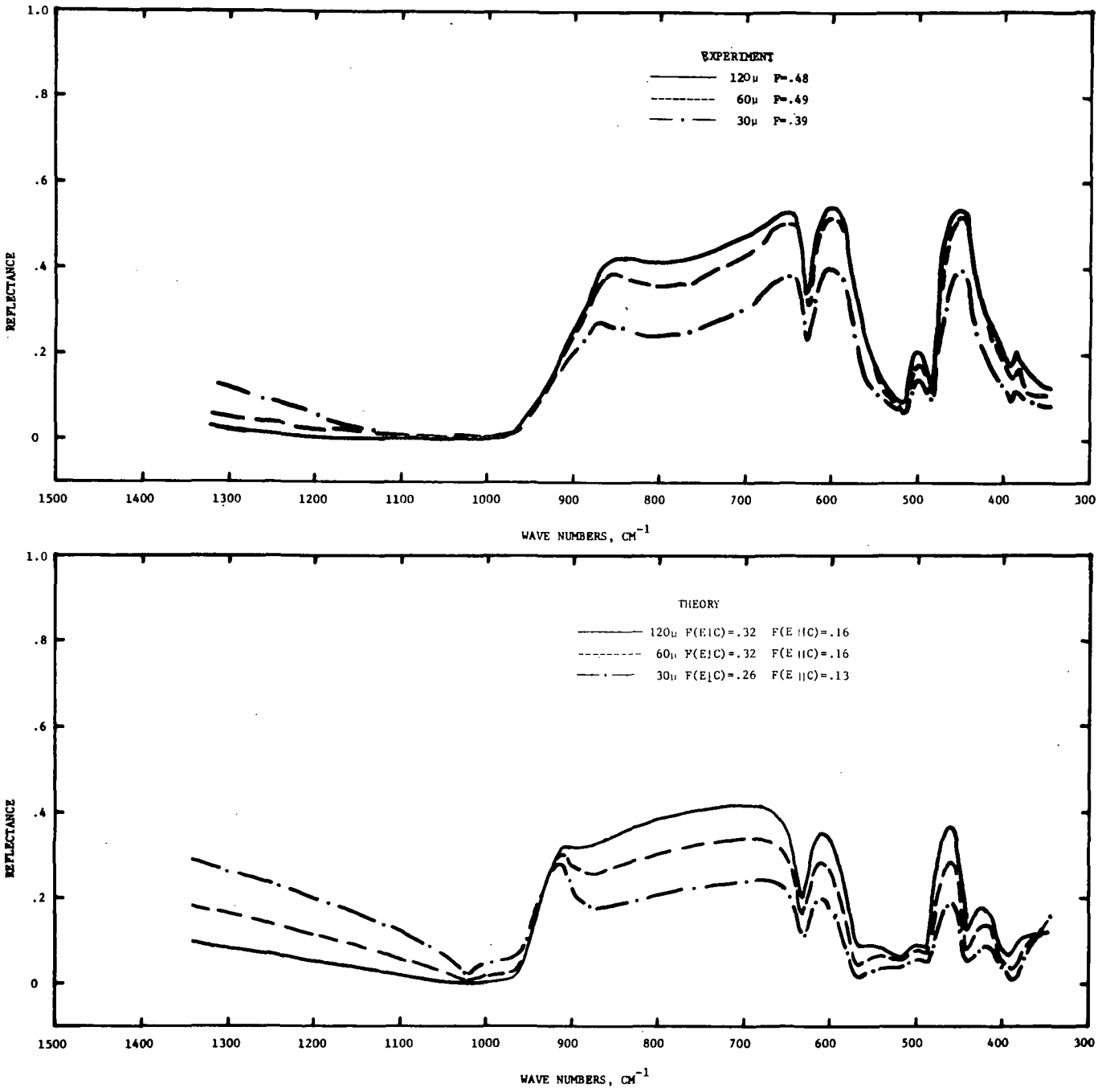


FIGURE 13 COMPARISON OF THEORETICAL AND EXPERIMENTAL REFLECTANCE OF CORUNDUM POWDERS

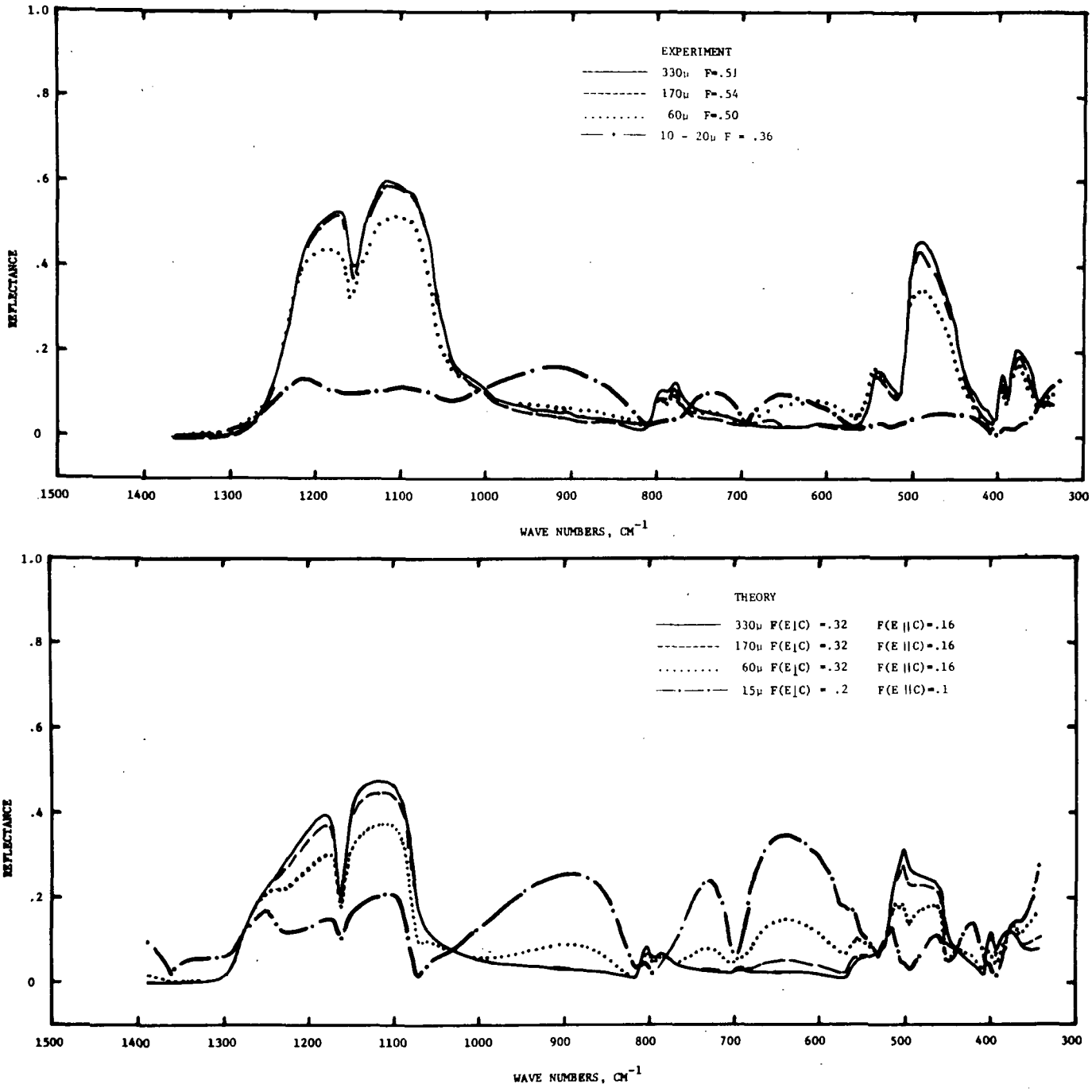


FIGURE 14 COMPARISON OF THEORETICAL AND EXPERIMENTAL REFLECTANCE OF QUARTZ POWDERS

shown in Figures 13 and 14 include the effects of edges but not of the surface asperities which are likely to dominate in large particle size corundum.

At the smallest particle size, the general level of the theoretical spectrum is higher than that observed experimentally. Further, as with corundum, the theoretical spectrum for small particle size shows a cusplike feature at the Christiansen frequency (1360 $cm^{-1}$ for quartz and 1020 $cm^{-1}$ for corudnum) not shown in the experimental results.

The higher level predicted by theory for small particles may be due to the experimental onset of other wave optical effects that have not been accounted for under conditions of the approximate equality of $d$ and $\lambda$. Alternatively the effect may be caused by aggregation effects which have not yet been included in the theory. The cusplike feature referred to above is removed by the corrections to the angular distribution of the scattering function discussed earlier. A preliminary set of theoretical spectra using the corrected coarse particle theory for corundum is shown in Figure 15. The curves were generated from a test program involving a limited number of spectral points and including only the $E \perp C$ orientation optical constants. Nonetheless, the cusplike feature has been shown to have been an artifact of the previous distribution function. The discrepancy between the particle size trend near 950 $cm^{-1}$ in these theoretical curves and the experimental results (Figure 13) is partly owing to the neglect of the $E \parallel C$ optical constants. However, this kind of feature did, in fact, also occur in the previous coarse particle theoretical treatments for the smaller particles. We attribute the effect to the same possible causes as those discussed above.

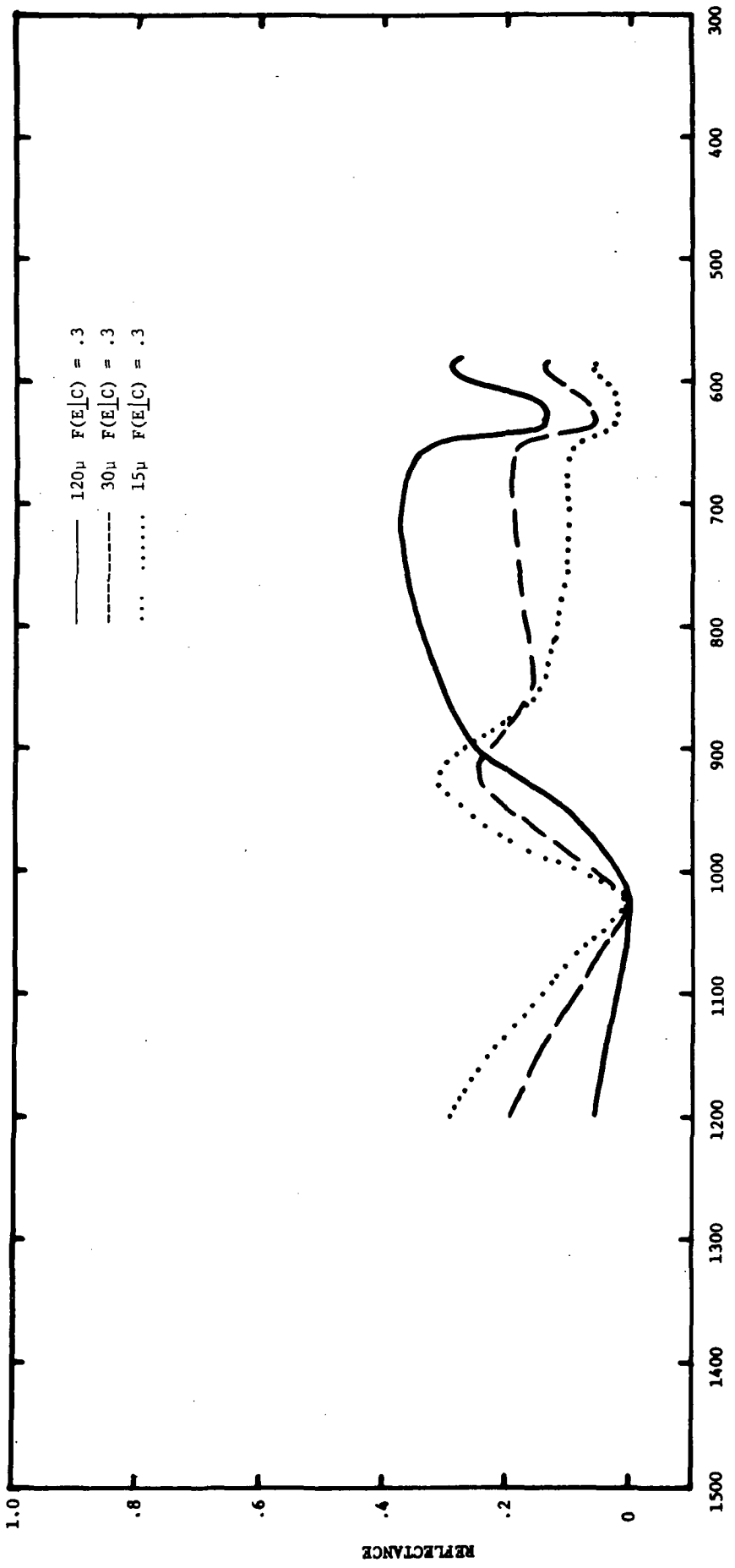


FIGURE 15 PRELIMINARY RESULTS OF MODIFIED THEORY FOR THE REFLECTANCE OF CORUNDUM POWDERS

## B. MIXTURES

The ultimate purpose of this work is to be able to decipher the spectrum of unknown mixtures of minerals. This inverse process depends critically on the validity of the mixing rule used. For the coarse particle theory our rule is

$$\frac{K}{S} = \frac{K_1 + K_2 + K_3 \ldots}{S_1 + S_2 + S_3 \ldots} \tag{37}$$

where the individual K's and S's refer to the volume absorption and scattering coefficients of the various components in the powder, under the existing packing conditions.

A comparison of the spectrum of a "3:2" mixture of relatively coarse quartz and corundum powders and the theoretically derived result is shown in Figure 16. This spectrum is a repeat run on the mixture which gave the puzzling results shown in Figure 29 of our last report[1]. The present good agreement between theory and experiment encourages us to believe that the problem of spectral analysis is indeed feasible. We have previously pointed out in Figure 8 of ref (2), however, that even a linear mixing rule using the reflectance of the components is approximately valid for large opaque particles such as those used in this experiment since only the uppermost layer of particles is important in this case. It is worth noting that to a similar approximation our theory reduces to a linear reflectance mixing rule under these conditions.

It is clearly desirable to test our theory in the case of mixtures of smaller size particles for which our non-linear mixing rule would be required. The results of Adams and McCord[9] given in their Figure 4 show the results of non-linear mixing. The distinct curvature of their reflectance vs weight percent plots is in general agreement with the mixing rule given by equation (37).

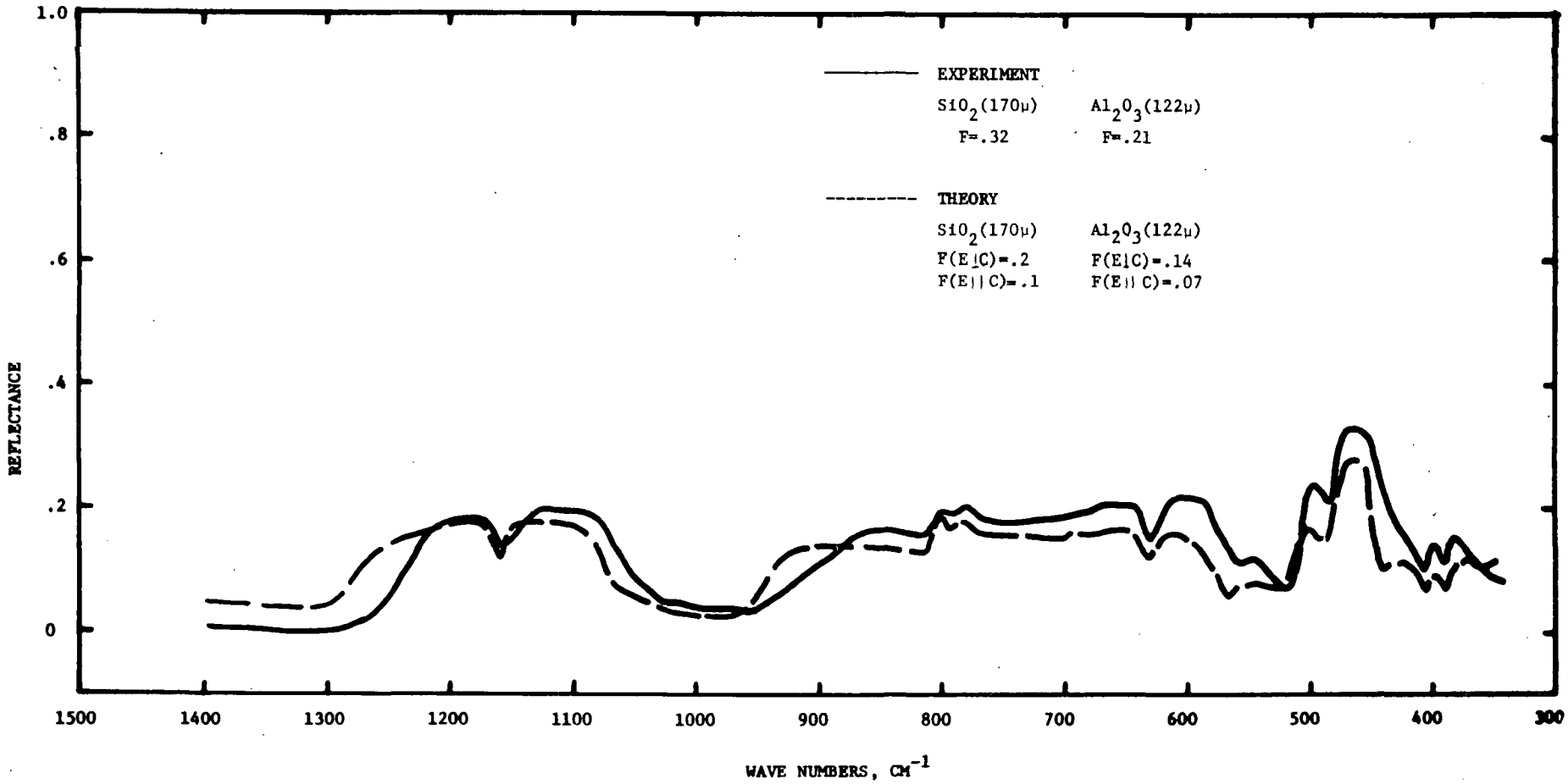


FIGURE 16 REFLECTANCE OF A MIXTURE OF CORUNDUM AND QUARTZ POWDERS

A detailed comparison of the results of the spectra of the several mixtures we have run is not shown here for two reasons. First, as indicated by the variability in the spectrum of the "3:2" mixture it is very difficult to establish the actual mixing ratio in the effective radiating layer at the surface of the powder. Second, the Christiansen technique is necessarily invalid for a mixture as it is almost impossible for two powders to have a common Christiansen frequency, and our thermocouple technique is not as yet a sufficiently satisfactory substitute when close comparisons are required.

In view of the prevalence of glass particles in the lunar soils returned by the Apollo program, we felt it would be interesting to obtain a spectrum of a mixture of glass beads and powdered quartz. It is shown in Figure 17. We have redrawn the spectra of the separate components on the same figure for purposes of comparison. The principal effect of the glass beads is to markedly reduce the reststrahlen features of the quartz spectrum. Some broadening of the reststrahlen features of quartz can also be observed due to the broad character of the features of the glass spectrum. This is a general effect for amorphous materials.

It is interesting that in the relatively transparent region from 500 $cm^{-1}$ to 1000 $cm^{-1}$ (discounting the feature near 800 $cm^{-1}$) the resultant spectrum of the mixture does not lie between the levels of the spectra of the separate components. This phenomenon has been observed by others[10]. This minor effect is not explained by our current theory, but suggests that the present contact factor[1] may require modification so as to increase its effects.

## C. BLACKBODY STANDARDS

In our previous report we noted that certain spurious spectral features were probably caused by the 3M Nextel black paint with which our 30° V groove aluminum standards were painted. We began the current

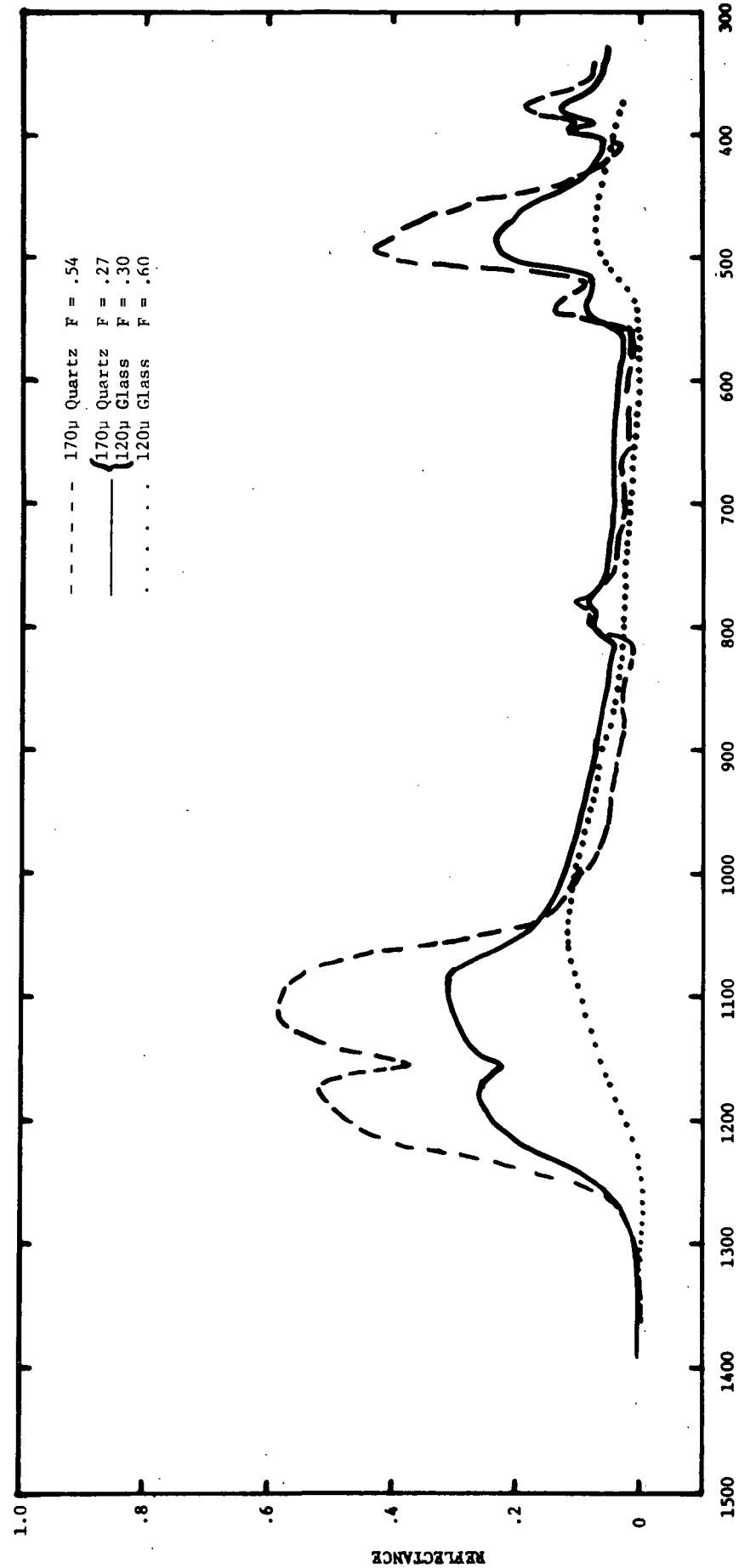


FIGURE 17 REFLECTANCE OF A MIXTURE OF QUARTZ AND GLASS POWDERS

experimental program with a set of experiments designed to ameliorate this difficulty. We made emission measurements on our previous standard and a duplicate sample coated with Parsons black paint (Eppley Laboratory). In addition, a Cabot Corporation, Carbolac 1 black powder sample (9mμ carbon particles) in the form of a powder bed was run in the usual manner of our powder samples. These three runs were intercompared and the spurious spectral features were clearly shown to be caused by the Nextel paint, which contains a large volume of glass spheres. Figure 18 shows the results of comparing the 3M black coated sample and the one coated with Parsons black. These data indicate a minimum emittance of .92 for the 1090 $cm^{-1}$ feature (referred to the Parsons black standard). The result is in reasonable agreement with the .89 value given by the National Bureau of Standards[11] considering the emittance enhancing effect of the V grooves. Sparrow[12] shows a theoretical enhancement of a .9 emittance to slightly over .96 by perfect 30° V grooves for a diffusely reflecting material. The results of the runs on the Carbolac black powder and the Parsons black standard indicate flat spectral responses from 500 $cm^{-1}$ to 1400 $cm^{-1}$. However, the Parsons "blackbody" emittance appears to fall monotonically at lower frequencies reaching apparent values of about .97 near 350 $cm^{-1}$. This trend is in accord with some specular data given by a U. S. Department of Commerce Report[13]. As the usual temperature measurement problems occur in the use of the Carbolac powder and as our principal interest is in the spectral shapes for our various curves, we have chosen to use the Parsons coated "blackbody" as the standard for our present work. This should introduce only very small errors in the absolute values of our measurements and a small slope at the lowest frequencies. Therefore all of our past data were recalibrated using the apparent emittance of the 3M black standard as the calibrating factor. This change of standard has removed several puzzling discrepancies between theory and experiment noted in our previous work.

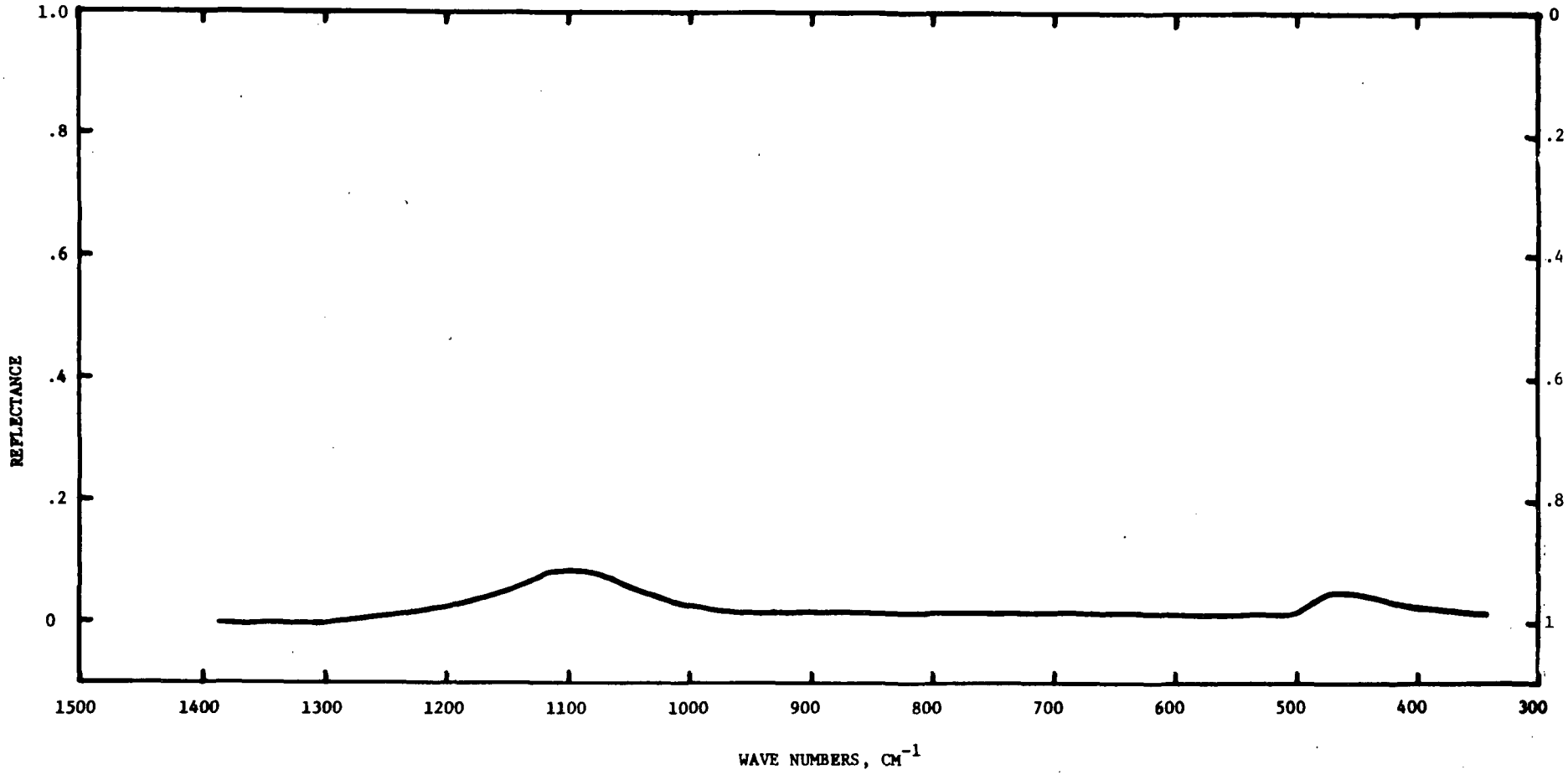


FIGURE 18 COMPARISON OF 3M AND PARSONS BLACK PAINTS

## VII. THE EFFECT OF TEMPERATURE GRADIENTS

In our previous report we attempted to determine the effects of temperature gradients on the emittance spectra of the powders by carrying out a set of measurements at differing gas pressures. The results were somewhat inconclusive owing to the very noisy character of the spectra at that time. The noise that occurred under vacuum conditions resulted from the low sample surface temperature arising from the combination of the large sample depth and the low thermal conductivity of the powder. Our apparatus did not permit us to raise the heater temperature sufficiently to overcome these factors. In order to remedy this difficulty we simply reduced the depth of our sample tray which is quite acceptable as the optical depth in these powders is always quite small. The new sample tray is .6 cm deep (as opposed to 1.1 cm previously) and the differential thermocouples are stationed .2 and .5 cm above the base. The new tray has also been reduced in diameter so that its volume is now 3.04 $cm^3$ instead of 11.58 $cm^3$.

As a result of the altered depth of the tray it is now quite easy to obtain a surface temperature of the order of $10^{o}K$ in excess of the temperature of the surrounding cavity. This temperature difference reduces the noise to an acceptable level and the results of repeating the previous experiment are shown in Figure 19. The improved experimental setup removes the source of the spurious fine structure of the previous experiment and now shows a consistent trend of the emittance in the two relatively transparent spectral regions near 700 $cm^{-1}$ and 900 $cm^{-1}$. It should be observed that there is a small trend in the opposite direction for the opaque spectral regions in the vicinity of 1100 $cm^{-1}$ and 1200 $cm^{-1}$. The other opaque region near 500 $cm^{-1}$ shows no apparent effect. As usual these curves have been fitted to surface temperatures given by the Christiansen[3,7] technique with the emittance taken to be unity at 1360 $cm^{-1}$. The surface temperature derived by linear extrapolation of the temperatures obtained from our thermistor in the base and the differential thermocouples immersed in the powder exceeds the

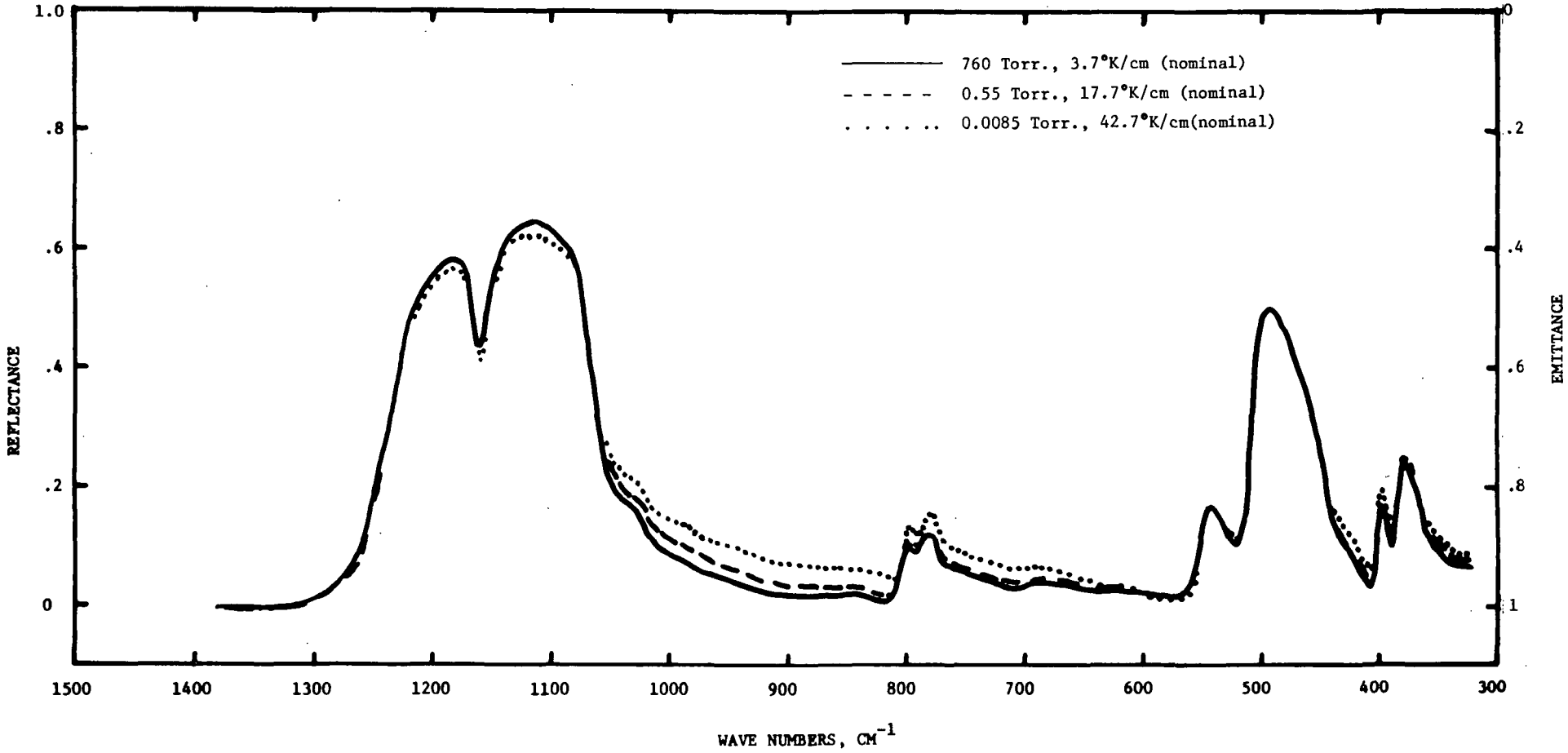


FIGURE 19 REFLECTANCE OF 330μ (F = .61) QUARTZ POWDER: THE EFFECT OF AMBIENT PRESSURE

temperature obtained by the Christiansen technique by the large value of $16^{o}$ under the vacuum conditions. Under atmospheric pressure the two temperatures differ by about $1^{o}$ in this experiment. In general, the temperature difference for atmospheric pressure experiments averages $.5^{o}$ and may be zero under favorable experimental conditions.

In order to test the likelihood that the temperature gradient depends on the particle size owing to different relative contributions of the radiative and conductive conductivities, we ran the same kind of experimental set for 60μ quartz powder. The results are shown in Figure 20. The temperature obtained from linear extrapolation of the thermal measurements differs again in this case by about $16^{o}$ from the Christiansen temperature at the lowest pressure but is identical to it for the atmospheric pressure spectrum. Again, the same transparent regions show the same trends with pressure or temperature gradient. However, while the trends in several opaque regions are consistent within this one experimental set, they do not appear to change monotonically with pressure. Further, they differ from the results shown in Figure 19 for the opaque regions. It should be noted that the nominal gradients quoted on the figures are those derived from the thermal measurements assuming a linear relationship near the powder surface.

Referring first to the relatively transparent region between 600 $cm^{-1}$ and 1000 $cm^{-1}$ in these two figures, we note that the spectra for the highest gradient cases have the lowest apparent emittance (highest reflectance) and the trend is continuous up to the approximately isothermal spectra derived from atmospheric pressure measurements. This behavior is to be expected since the mean free path of the radiation should be less in this spectral region than at the Christiansen frequency. The effect is simply caused by normalizing the entire spectrum with respect to the Planck function appropriate to the Christiansen frequency at which the depth of origin of the radiation is the greatest and hence the effective temperature the highest. Therefore, while the apparent

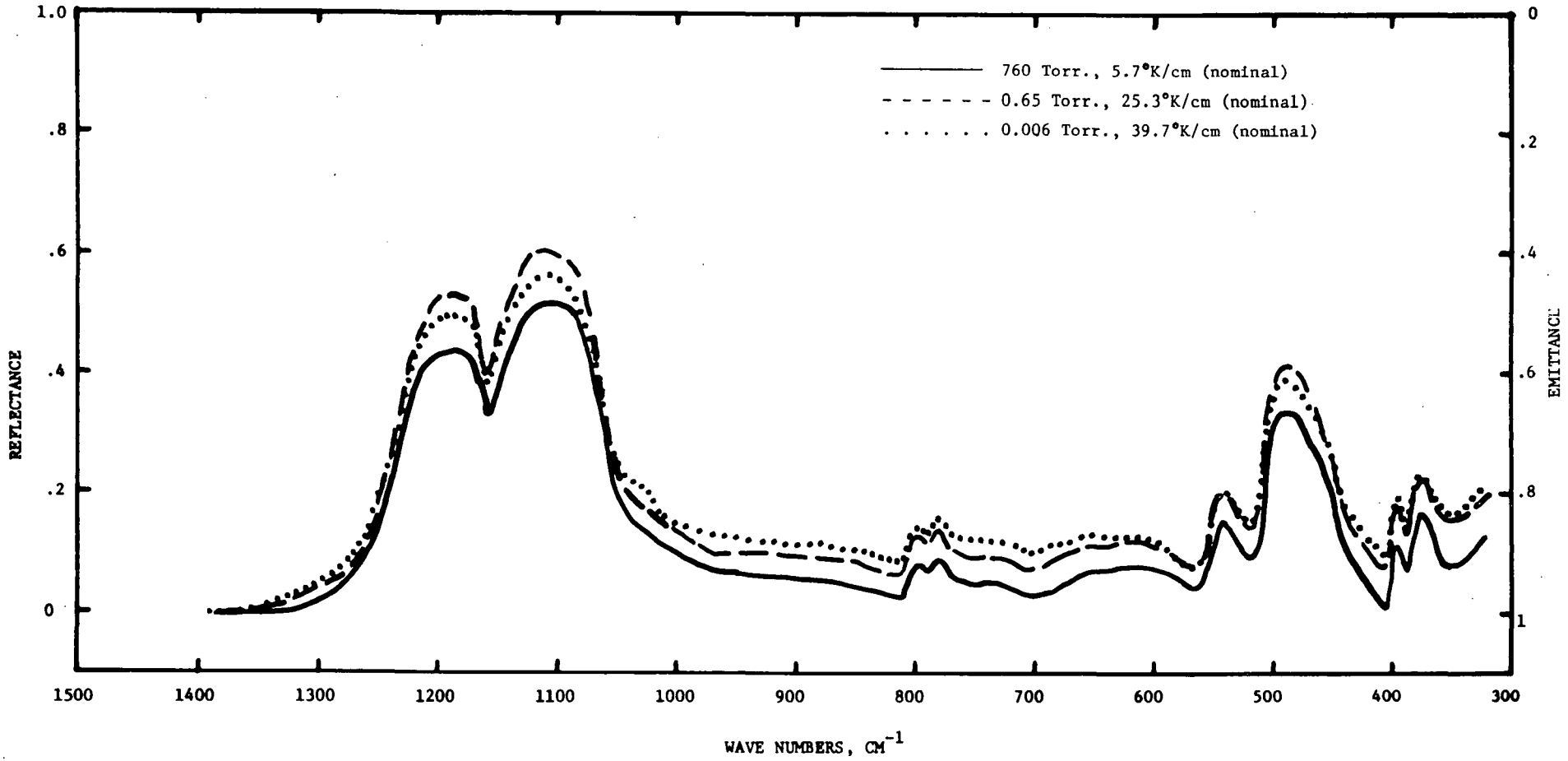


FIGURE 20 REFLECTANCE OF 60μ (f = .53) QUARTZ POWDER:
THE EFFECT OF AMBIENT PRESSURE

emittance is correct at the Christiansen frequency, it is too low elsewhere. The steeper the gradient, the greater is the effect.

The same considerations should apply to the opaque regions for which the Planck function used departs to the greatest degree from the proper Planck function characteristic of the surface temperature. The intermediate pressure case (upper curve in the opaque regions) shown in Figure 20 is in accord with this trend in as much as the apparent discrepancy with respect to the solid curve is still greater here than in the transparent regions. However, we are puzzled by the apparent reversal of this trend for the spectrum obtained at the lowest pressure. It is to be noted that the departures from the solid curve are comparable in the opaque and relatively transparent regions which further raises some questions with regard to the validity of this curve.

In Figure 19 this difficulty is further accentuated in the opaque regions in that the steep gradient curve is superimposed on the base curve at 500 $cm^{-1}$ and is actually on the reverse side in the 1100 $cm^{-1}$ and 1200 $cm^{-1}$ regions. For this experiment the powder surface slumped during the course of the experiment by about .1 cm and this fact resulted in the higher volume fraction noted on the figure and may have contributed to the $1^{o}$ difference between the measured temperature and the Christiansen temperature for the atmospheric pressure spectrum. A comparison of the atmospheric pressure spectrum with that shown in Figure 14 indicates that the emittance level has changed. Thus either the changed volume fraction has an unsuspected effect for this very large particle size or the results are in error.

We have mentioned that the temperature determined by the Christiansen technique differs by as much as $16^{o}C$ from that determined by linear extrapolation of the temperatures measured by the sensors in the powder and tray. The sign of the temperature difference is such that the Christiansen temperature is the lower, which appears to be quite unreasonable. In an attempt to understand this problem we have considered the possibility that the temperature distribution is, in fact, nonlinear

owing to the contribution of radiant heat transfer to the overall thermal conduction. We have therefore assumed an expression of the form

$$T^4 + a\,T = b - cx \tag{38}$$

for the dependence of the absolute temperature T on the distance x measured from the bottom of the sample tray (a, b, and c are constants). We have fitted this formula to the measured temperatures at the base of the tray and in the powder and extrapolated the equation to the surface. The results show a small curvature in the case of the atmospheric pressure data and a larger curvature for the cases of steeper temperature gradients. However, the surface temperature so derived for the steepest gradient case is still considerably higher than the Christiansen temperature. Thus it appears that even a $T^4$ contribution is insufficient to explain the discrepancy. It is, indeed, very likely that within a few photon mean free paths of the surface, T must vary exponentially rather than like $x^{1/4}$. This type of behavior is shown by equations (B4) and (B5) of our previous report[1] (owing to a typographical omission each of these equations lacked the term $+B_s'x$ on their right-hand sides). Further consideration of this question should be undertaken.

In our previous report[1] we have derived an expression for the emittance correction required in the presence of a significant temperature gradient:

$$\Delta\epsilon_s = \frac{(2-\epsilon_s)}{K + 2S} \quad \frac{\left(\frac{dT}{dx}\right)_s}{(T_s - T_b)} \tag{39}$$

where x is here considered to be measured inward from the surface of the powder, and the subscript s refers to quantities evaluated at the surface of powder. The true emittance $\epsilon_s$ is related to the apparent emittance $\epsilon_s'$ by the relation

$$\epsilon_s = \epsilon_s' - \Delta\epsilon_s \tag{40}$$

The calculation of $\Delta\epsilon_s$ from (39) can in principle be carried out by an iterative procedure without prior knowledge of $T_s$ and $(dT/dx)_s$. First we would assume a trial value of $T_s$ and from the Planck function at this temperature calculate the apparent emittance $\epsilon_s'$ from the measured radiance of the sample. We would next derive the value of the surface gradient $(dT/dx)_s$ which from (39) and (40) makes $\epsilon_s = 1$ at the Christiansen frequency. We would then use (39) and (40) to calculate $\epsilon_s$ over the whole spectrum. If the original selection of $T_s$ were correct this calculated emittance spectrum should agree with the spectrum of the powder determined experimentally under conditions of small temperature gradient e.g., at atmospheric pressure. If not, a new starting temperature, based on the sign of the discrepancy, would be selected and the iteration continued until satisfactory agreement with the zero-gradient spectrum is obtained over the whole spectrum. If all goes well the procedure should allow one to determine both $T_s$ and $(dT/dx)_s$ and to gain valuable insight into the radiative transfer mechanism.

As an approximation to this technique we have attempted to simply use the Christiansen method to provide the starting temperature, and making use of equations (39) and (40) have tried to ascertain whether the apparent emittance difference between spectra of large and small gradients would vanish without iteration. The values of K and S were taken from our theoretical model. The results of using this approximation were not satisfactory. The trouble may lie in the approximation, the absolute values of K and S (as only their ratio is required for the reflectance calculations) or experimental errors. We intend to examine these various possibilities in more detail as a good method of obtaining the gradient is desirable. However, we should note that none of these problems bears significantly on the problem of determining mineral compositions as the effects can be seen in Figures 19 and 20 to be relatively small.

## VIII. CONCLUSIONS

The major result of the present study is that particle asperities (especially edges) play an essential role in producing the observed spectra of mineral powders when the particle size is equal to or greater than the radiation wavelength. The incorporation of the effect of edges has greatly improved the fit between theory and experiment in several ways. It has provided a mechanism whereby the observed trend of emittance with particle size in relatively opaque regions of the spectrum is well accounted for without altering the previously attained agreement in semitransparent regions. Further, the hitherto puzzling "scallop" region, notably existing in the spectrum of corundum, can be accounted for by the same mechanism. We feel the evidence is quite strong that the asperities known to exist on the surfaces of the corundum particles also contribute to the scallop and, indeed, must be the principal factor for the larger particles. The combination of the above particle size trend and the scallop effect has also served to provide good agreement with the absolute experimental emittance level.

A great improvement in the fit between the spectral level predicted by the fine particle theory and experimental results has been obtained by applying the theory to experiments with particles of a much reduced size. A better fit is obtained for powders in which the aggregation effects have apparently been reduced. This is quite reasonable as the effects of particle aggregation are not as yet included in the theory.

A further experimental study of the effects of temperature gradients on the emission spectra has been included. The refined experimental technique has greatly improved the signal-to-noise ratio under vacuum conditions. The data indicate the likelihood of a very large temperature gradient near the surface of particulate samples under vacuum conditions.

As a result of the improvements obtained in the theory, we now believe that a beginning can be made on the inverse problem of spectral analysis of an unknown mixture of minerals.

## IX. SUGGESTIONS FOR FUTURE WORK

We believe that future work should include the following topics.

1. A computer study of the inverse problem of analysis of a mixture of minerals.

2. Further refinements in the coarse-particle theory such as the use of the improved angular distribution function and the inclusion of the effects of surface asperities discussed in this report.

3. The measurement of the emittance spectra of sapphire spheres to further test the validity of the asperity hypothesis.

4. Refinement of the fine-particle theory to distinguish the importance of surface and volume reflectance, and to include the effect of particle aggregation.

5. Experimental measurements relating to topic (4) such as a specular reflectance measurement of a fine particle sample prepared by settling in a liquid.

6. A test of the proposed iteration method for data reduction in the case of steep thermal gradients such as those discussed in this report.

## X. REFERENCES


1. J. R. Aronson, A. G. Emslie, L. H. Roach, P. F. Strong and P. C. vonThüna, "Development of a Theory of the Spectral Reflectance of Minerals, Part II," Report to NASA, Manned Spacecraft Center, April 1971 (Contract NAS9-10875).

2. J. R. Aronson, A. G. Emslie, R. V. Allen and H. G. McLinden, J. Geophys. Res. 72, 687 (1967).

3. J. E. Conel, J. Geophys. Res 74, 1614 (1969).

4. H. C. van de Hulst, Light Scattering by Small Particles, (John Wiley and Sons, Inc., New York, 1957).

5. R. G. Giovanelli, Austr. J. Phys. 10, 227 (1957).

6. A. S. Barker, Jr., Phys. Rev. 132, 1474 (1963).

7. J. R. Aronson, A. G. Emslie, T. P. Rooney, I. Coleman and G. Horlick, Appl. Opt. 8, 1639 (1969).

8. J. R. Aronson and A. G. Emslie, "The Influence of Physical Variables on Spectral Signatures of National Targets," Report to AFCRL, Dec. 1969 (Contract F19628-67-C-0353).

9. J. B. Adams and T. B. McCord, Science 171, 567 (1971).

10. E. A. Schatz, J. Opt. Soc. Am 57, 941 (1967).

11. Private communication from V. Weidner, National Bureau of Standards.

12. E. M. Sparrow and R. D. Cess, Radiation Heat Transfer, (Brooks/Cole Publishing Co., Belmont, California, 1966), p. 169.

13. W. Y. Ramsey, Meteorological Satellite Laboratory Report No. 31, U. S. Department of Commerce, April 1964, AD No. 446291.

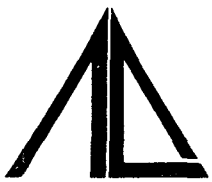

CAMBRIDGE,
MASSACHUSETTS

CHICAGO
NEW YORK
SAN FRANCISCO
WASHINGTON
ATHENS
BRUSSELS
CARACAS
LONDON
MEXICO CITY
PARIS
RIO DE JANEIRO
TORONTO
ZURICH